Heliyon 9 (2023) e15963

Contents lists available at ScienceDirect

Heliyon

journal homepage: www.cell.com/heliyon

Research article

A strategy for low-cost portable monitoring of plasma drug concentrations using a sustainable boron-doped-diamond chip

Takuro Saiki [a], Genki Ogata [b], Seishiro Sawamura [c], Kai Asai [b], Olga Razvina [d], Kota Watanabe [e], Rito Kato [e], Qi Zhang [c,f], Koei Akiyama [c,g], Sasya Madhurantakam [c], Norzahirah Binti Ahmad [c], Daisuke Ino [c], Haruma Nashimoto [h], Yoshifumi Matsumoto [a], Masato Moriyama [a], Arata Horii [f], Chie Kondo [i], Ryosuke Ochiai [i], Hiroyuki Kusuhara [h], Yasuo Saijo [a], Yasuaki Einaga [b], Hiroshi Hibino [c,j,*]

[a] *Department of Medical Oncology, Niigata University Graduate School of Medical and Dental Sciences, 1-757 Asahimachi-dori Chuo-ku, Niigata, Niigata 951-8510, Japan*
[b] *Department of Chemistry, Keio University, 3-14-1 Hiyoshi, Yokohama, Kanagawa 223-8522, Japan*
[c] *Division of Glocal Pharmacology, Department of Pharmacology, Graduate School of Medicine, Osaka University, 2-2 Yamadaoka, Suita, Osaka 565-0871, Japan*
[d] *G-MedEx Project, Niigata University Graduate School of Medical and Dental Sciences, 1-757 Asahimachi-dori Chuo-ku, Niigata, Niigata 951-8510, Japan*
[e] *Niigata University School of Medicine, 1-757 Asahimachi-dori Chuo-ku, Niigata, Niigata 951-8510, Japan*
[f] *Department of Otolaryngology Head and Neck Surgery, Niigata University Graduate School of Medical and Dental Sciences, 1-757 Asahimachi-dori Chuo-ku, Niigata, Niigata 951-8510, Japan*
[g] *Department of Molecular Physiology, Niigata University Graduate School of Medical and Dental Sciences, 1-757 Asahimachi-dori Chuo-ku, Niigata, Niigata 951-8510, Japan*
[h] *Laboratory of Molecular Pharmacokinetics, Graduate School of Pharmaceutical Sciences, The University of Tokyo, 7-3-1, Hongo, Bunkyo, Tokyo 113-0033, Japan*
[i] *Pharmaceuticals and Life Sciences Division, Shimadzu Techno-Research, Inc., 1, Nishinokyo-shimoai-cho, Nakagyo-ku, Kyoto, Kyoto 604-8436, Japan*
[j] *AMED-CREST, AMED, Osaka 565-0871, Japan*

ARTICLE INFO

Keywords:
(Alphabetical order): Boron-doped diamond
Clinical samples
Drug monitoring
Electrochemistry
Plasma concentration
Portable system
Sustainability

ABSTRACT

On-site monitoring of plasma drug concentrations is required for effective therapies. Recently developed handy biosensors are not yet popular owing to insufficient evaluation of accuracy on clinical samples and the necessity of complicated costly fabrication processes. Here, we approached these bottlenecks via a strategy involving engineeringly unmodified boron-doped diamond (BDD), a sustainable electrochemical material. A sensing system based on a ~1 cm^2 BDD chip, when analysing rat plasma spiked with a molecular-targeting anticancer drug, pazopanib, detected clinically relevant concentrations. The response was stable in 60 sequential measurements on the same chip. In a clinical study, data obtained with a BDD chip were consistent with liquid chromatography–mass spectrometry results. Finally, the portable system with a palm-sized sensor containing the chip analysed ~40 μL of whole blood from dosed rats

* Corresponding author. Division of Glocal Pharmacology, Department of Pharmacology, Graduate School of Medicine, Osaka University, 2-2 Yamadaoka, Suita, Osaka 565-0871, Japan.
E-mail address: hibino@pharma2.med.osaka-u.ac.jp (H. Hibino).

https://doi.org/10.1016/j.heliyon.2023.e15963
Received 26 July 2022; Received in revised form 20 April 2023; Accepted 27 April 2023
Available online 9 May 2023

within ~10 min. This approach with the 'reusable' sensor may improve point-of-monitoring systems and personalised medicine while reducing medical costs.

1. Introduction

Measurement of plasma concentration of drugs – in particular, those with a narrow therapeutic window – at designated intervals is necessary for optimising dosage regimens for individual patients [1,2]. Currently, in clinical trials and in clinical practice, most drugs are detected by an immunoassay or liquid chromatography−mass spectrometry (LC−MS). The measuring instruments for these methodologies are too expensive for small- and medium-sized hospitals and clinics. In addition, LC−MS requires well-trained personnel. Therefore, in many cases, plasma samples are delivered to and analysed by third parties. Because this outsourcing takes a long turnaround time of several days to a few weeks and is costly, it is difficult to modify a therapeutic protocol for each patient in real time with reference to actual drug concentrations in plasma. Such disadvantages are hurdles for disseminating 'therapeutic drug monitoring' (TDM) as a standard of medical care to resource-limited areas, including local communities with small population and developing countries [3,4]. Notably, TDM is economically impactful; the global market size was valued at US$2.2 billion in 2021 and is expected to reach US$3.5 billion by 2028 (https://precisionbusinessinsights.com/market-reports/global-therapeutic-drug-monitoring-market/).

To address these bottlenecks, a variety of biosensors suitable for portable or on-site drug monitoring were recently created. For example, an immunoassay using an advanced label of near-infrared fluorescent dye detects an immunosuppressant, mycophenolic acid, with a limit of detection (LOD) of 2.5 nM and a dynamic range of 5.3–121.7 nM in human plasma [5]. The surface plasmon resonance sensor employing a DNA aptamer can measure the concentration of an antineoplastic drug, irinotecan, with a high selectivity in a range of 0.2–12.8 μM [6]. More excellent sensitivity is described in a surface-enhanced Raman spectroscopy method with a direct anticoagulant, edoxaban, (limit of quantification: 1 pM) [7]. An electrode based on $CeBiO_x$ nanofiber detects acetaminophen with a low detection limit of 0.2 μM [8]. Furthermore, a sensor combining a molecularly imprinted polymer with an electrochemical electrode can separately quantify the antibiotics ceftazidime and avibactam in clinical samples [9]. Nevertheless, these devices have not yet been actually translated to routine clinical applications owing to the following problems. First, it is essential for the devices to be tested for sensor-to-sensor variability, and it is necessary to quantitatively compare the measurements in real-world samples from patients to the results of current gold standard methods, but there are limited number of studies where 'both' evaluations have been performed [10]. The second reason is related to the design of advanced sensors; most of them are constructed from a combination of drug-recognizing bioreceptors such as specific antibodies, enzymes, DNA aptamers, and molecularly imprinted polymers, along with an electrochemical or optical platform converting a biological response to a quantifiable signal [5,6,9,11–14]. Processes for the identification, fabrication, optimisation, and integration of these components likely require much effort and complex techniques and therefore will necessitate considerable expenditures and turnaround time. Third, as for low-invasiveness watch-type and microneedle-type wearable sensors [15,16], they detect a drug in sweat and in dermal interstitial fluid, thereby raising questions whether and how the drug fraction detectable in these matrices mirrors the plasma concentration [10].

Another key issue of TDM is that in plasma, 'total drug concentration', which is the sum of a protein-bound fraction and a protein-unbound (free) fraction, is currently measured and interpreted in terms of pharmacokinetic principles and relevant clinical parameters [17]. Accordingly, less expensive systems for rapid and easy determination of a total concentration are in demand. To address this issue and the problems mentioned above, in this study, we propose an electrochemical approach involving a boron-doped diamond (BDD) electrode without any engineering modifications. The electrochemical method analyses electrical properties generated by movement of electrons from one element to another in a reaction, called redox or oxidation-reduction reaction. As compared to conventional materials such as carbon, gold, and platinum, BDD is characterised by a wide potential window for water stability, a low capacitive current, high repeatability of the measurement, and high resistance to non-specific absorption [18–20]. In the analytical systems we constructed, a small BDD chip of ~1 cm^2 serves as a drug sensor. As a test compound, we chose multi-kinase inhibitor pazopanib, a molecular-targeting anticancer drug whose TDM is thought to be clinically effective [21,22]. To the best of our knowledge, this compound has not been fully characterised by electrochemical approaches. When plasma samples from orally dosed healthy rats and patients with sarcoma were analysed in our tabletop system, the estimated concentrations approximately matched the values determined by LC coupled with tandem mass spectrometry (MS/MS). Not only did the BDD chips demonstrate a significantly high level of quantitativity, but they also exhibited excellent measurement repeatability. Moreover, we examined the reproducibility of results among different chips. Notably, these three evaluation tests are not addressed by a recently developed BDD-based biosensor, which is deposited with graphite on the surface and thereby could be more costly and time-consuming than our engineeringly unmodified chips [23]. Finally, we developed a prototype of a handy monitoring system equipped with a handheld-type biosensor. This system, which may be useable in laboratories of regular hospitals and clinics, successfully determined drug concentration in plasma from a small aliquot of whole blood, ~40 μL, within a short sampling-to-result time: ~10 min. A bioreceptor-free BDD chip is reusable and easy to handle, has a low production cost, and theoretically can detect a wide variety of drugs by simply modifying the electric-potential protocol. Consequently, the strategy described in this study may contribute to advances in point-of-monitoring systems and reduction of the cost for TDM worldwide.

2. Results

2.1. Basic experiments with BDD chips in a tabletop system

2.1.1. Electrochemical characterisation of pazopanib

Initially, we examined the basic electrochemical profile of pazopanib by means of plate electrodes made of different materials such as diamond doped with 1% or 10,000 ppm boron (i.e. BDD), conventional glassy carbon, or platinum, in a tabletop system composed of a sensing element, potentiostat, and desktop computer (Fig. 1). In the sensing element, a square-shaped chip of each electrode (~1 cm^2) without any pre-treatment was overlaid with a small cylindrical chamber that has a circular hole at the bottom (volume of the applied sample: 120 μL; the hole diameter: 6 mm; electrochemically reactive surface area: ~28 mm^2; Supplementary Fig. S1). All the BDD chips used in this study (chip IDs: A–J) were derived from the same wafer plate (see Methods). Cyclic voltammetry with a BDD chip (chip ID: A) in phosphate-buffered saline (PBS) containing 300 μM pazopanib clearly indicated – as compared to the response in PBS alone – two different current components: an anodic current that was evoked at >0.7 V (versus Ag/AgCl) and a cathodic current that began at −0.2 V and gradually increased as the potential was shifted in the negative direction (Fig. 1a). A glassy-carbon chip elicited a similar anodic current but barely detected the cathodic current (Fig. 1b). Hardly any drug response was observed with a platinum chip (Fig. 1c). Plasma, which is in general employed for TDM, contains large amounts of endogenous substances including albumin, ascorbic acid, and uric acid, which induce a marked current at positive potentials over ~0.25 V [24–26]. This current likely interferes with the anodic current resulting from pazopanib. Overall, because in the pazopanib-containing solution, the BDD chip yielded a clear-cut current at negative voltages (Fig. 1a), this material was most suitable for the purpose in this study.

Additional experiments revealed two patterns [1]: induction of the cathodic current from pazopanib requires an oxidised form, which is generated by the potential protocol used in Fig. 1a (Supplementary Fig. S2a), and [2] the cathodic current was detectable on the electrode chip with an oxygen (O)-terminated surface but not with a hydrogen (H)-terminated surface (Supplementary Fig. S2b). To address the latter issue, a pre-treatment potential protocol for O termination – i.e. initial potential 0 V, stepping to 1.0 V for 5 s, stepping to −1.0 V for 20 s, and holding at 1.0 V for 60 s – was applied in advance to BDD chips in all the following electrochemical experiments.

2.1.2. Optimisation of the potential protocol for the measurement of pazopanib levels in rat plasma

Next, we tested whether a BDD chip (chip ID: C) could detect pazopanib dissolved in plasma collected from a Wistar rat (Fig. 2). When plasma alone was analysed, the cyclic voltammogram showed a significant anodic current at potentials exceeding 0.2 V and a cathodic current similar to the current recorded in PBS alone. Addition of pazopanib (300 μM) increased both the anodic current and cathodic current, but the amplitudes were small (Fig. 2a). Therefore, we treated the test samples with acetonitrile to remove the endogenous proteins before electrochemical measurement (Fig. 2b; see 'Protocol 1' in Supplementary Fig. S3a). This procedure significantly reduced the anodic currents evoked at positive potentials in plasma samples with and without pazopanib; however, at negative potentials, the procedure strongly enhanced the drug-induced current. Accordingly, we decided to pre-treat all plasma samples with acetonitrile in the following assays. In addition, the observations in this series of experiments (Fig. 2) indicated that the electrochemical approach possibly detects the protein-unbound fraction of pazopanib and that the method with acetonitrile can analyse the 'total' fraction underlying clinically relevant pharmacokinetic principles and parameters [17]. In this context, the enhanced fraction of the response with acetonitrile treatment is likely to mirror protein-bound fraction. Note that in the assays of plasma alone, little current was detected at negative potentials in the presence and absence of acetonitrile (Fig. 2a and b). This observation indicates that the plasma contains negligible amounts of endogenous substances that evoke significant reduction reaction and can influence the cathodic current elicited from pazopanib. Therefore, application of the negative potentials to BDD chip is suitable for analysis of the drug.

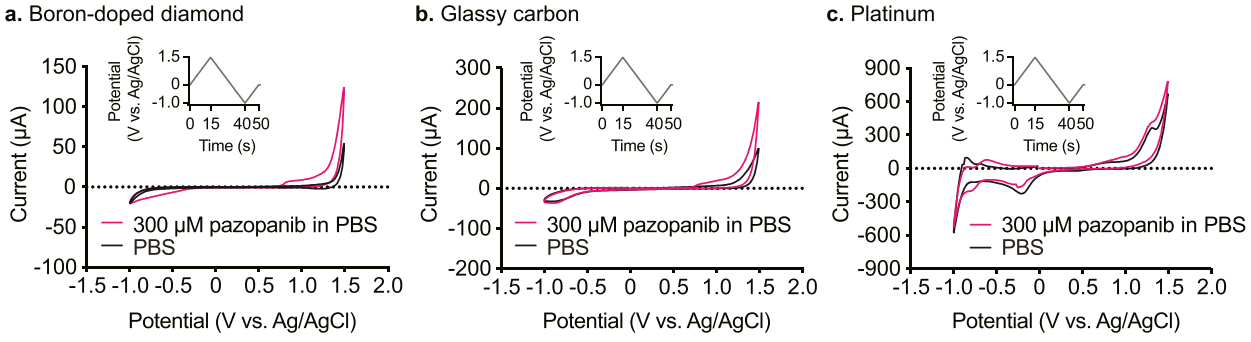

Fig. 1. Electrochemical analysis of pazopanib with plate electrode chips composed of different materials. The *panels* show cyclic voltammograms obtained with a plate-type electrode chip made of 1% boron-doped diamond (BDD) (*a*; chip ID: A), glassy carbon (GC) (*b*), or platinum (*c*). Each chip was set in a chamber of the tabletop measurement system illustrated in Supplementary Fig. S1. Phosphate-buffered saline (PBS) alone (*black curves*) or 300 μM pazopanib in PBS (*magenta curves*) was analysed by the potential protocol described in the *insets* (sweep rate: 0.1 V s^{-1}, potential window: −1.0 to 1.5 V, initial potential: 0 V versus Ag/AgCl).

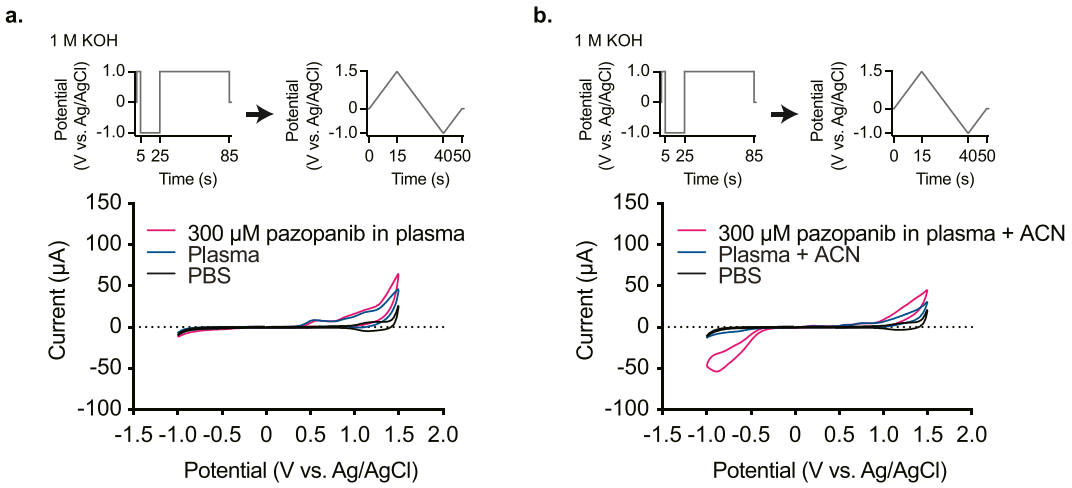

Fig. 2. Detection of pazopanib in rat plasma with a BDD chip. In this series of experiments, phosphate-buffered saline (PBS), plasma collected from a rat, and a rat plasma sample spiked with 300 μM pazopanib were assayed on a boron-doped diamond (BDD) chip (chip ID: C) in the tabletop system. The chip was pre-treated with a 1 M KOH solution via the potential protocol for oxygen termination of the surface (initial potential: 0 V vs Ag/AgCl, stepping to 1.0 V for 5 s, stepping to −1.0 V for 20 s, and holding at 1.0 V for 60 s), and was subjected to cyclic voltammetry (sweep rate: 0.1 V s^{-1}, potential window: −1.0 to 1.5 V, initial potential: 0 V versus Ag/AgCl) (for the protocols; see *insets*). Voltammograms of PBS alone, plasma alone, and plasma containing the drug are indicated by *black*, *blue*, and *magenta curves*, respectively. Although in *panel a*, plasma samples in the presence or absence of pazopanib were directly assayed on the chip, in *panel b*, the samples were treated with acetonitrile (ACN) to remove endogenous proteins prior to the electrochemical measurement (Supplementary Fig. S3a). (For interpretation of the references to colour in this figure legend, the reader is referred to the Web version of this article.)

Square wave stripping (SWS) voltammetry offers higher sensitivity and a broader dynamic range for measurement of analytes than cyclic voltammetry does [27]. Indeed, this notion was confirmed in PBS containing pazopanib by means of a BDD chip (Supplementary Fig. S4). Therefore, we selected SWS voltammetry for detecting pazopanib in plasma. Furthermore, in the processes of the sample preparation, not only the necessary volume of acetonitrile but also small aliquots of tetramethylammonium chloride (TMA; 10 mM) and sodium dodecyl sulphate (SDS; 1 M) were added to the samples in all the subsequent SWS voltammetric experiments (see 'Protocol 2' in Supplementary Fig. S3b). This arrangement was attributed to the reports that the supporting electrolyte, TMA, can reduce the resistance of the nonaqueous solution (i.e. acetonitrile) and SDS is likely to generate on the electrode surface a uniform negative charge film that enhances access of chemical compounds [28–30]. Our potential protocol for the electrochemical measurement consisted of four procedures (Fig. 3a); (i) step chronoamperometry for 'pre-conditioning' in a 1 M KOH solution for electrode surface O-termination (see Supplementary Fig. S2b), (ii) two cycles of cyclic voltammetry in PBS for 'quality control', which verifies whether the potential window of water stability and the baseline redox current are adequate, (iii) SWS voltammetry for the analysis of a plasma sample by the optimised potential protocol (deposition potential: 1.4 V, deposition time: 30 s, potential range: −0.8 to 0.4 V, ΔE: 50 mV, square-wave frequency: 10 Hz, and pulse amplitude: 50 mV), and (iv) step chronoamperometry for 'conditioning' in PBS, which likely removes fouling from the electrode surface and returns it to the initial state. Procedures (ii) to (iv) were repeated for sequential multiple-time measurements.

Fig. 3b shows a representative set of data from SWS voltammetry on a BDD chip (chip ID: D) with plasma samples spiked with pazopanib at different concentrations, from 0 to 150 μM, the range that covers the therapeutic window (43.3–97.1 μM) [31]. For this assay, the plasma was collected from the same rat (animal ID: Rt09). Initially, a sample without the drug was examined; the current relatively stabilised at −4 μA from ~0.3 to ~0 V and gradually enlarged as the applied potential was enhanced in the negative direction (0 to −0.8 V). When pazopanib-containing samples were tested, the latter current component got amplified in a concentration-dependent manner.

It was expected that in SWS voltammograms with plasma samples collected from different rats, the amplitudes of the baseline current evoked at ~0.3 to ~0 V would be inconsistent to some extent. In this context, when a calibration curve was obtained directly from the current amplitudes at some potential, the curve's property could vary among different individuals. To minimise this variation, we instead attempted to use slope values calculated from the current amplitudes at two separate potentials (ΔI/ΔV). Analysis of numerous combinations of the potentials revealed that the data at −0.35 V and −0.45 V ($\Delta I/\Delta V_{-0.35\ V;-0.45\ V}$) afforded a sensitive and stable calibration curve (Fig. 3b and see Figshare 1, https://doi.org/10.6084/m9.figshare.19313882, regarding protocol optimisation). Fig. 3c shows that plots of $\Delta I/\Delta V_{-0.35\ V;-0.45\ V}$ values at different drug concentrations (see Fig. 3b) were fitted to linear regression. Notably, this slope (Fig. 3c) significantly exceeded the slopes of the calibration curves obtained with the current amplitude at −0.35, −0.4, −0.45, −0.6, and −0.8 V (Supplementary Fig. S5).

Next, with a different BDD chip (chip ID: E), we evaluated measurement stability (Fig. 3d). The plasma sample containing either 10 or 50 μM pazopanib was alternately applied to the chip in the chamber 30 times each, and SWS voltammetry was carried out in every trial. $\Delta I/\Delta V_{-0.35\ V;-0.45\ V}$ values at each concentration were highly stable and similar to their mean values (13.92 for 10 μM and 20.54

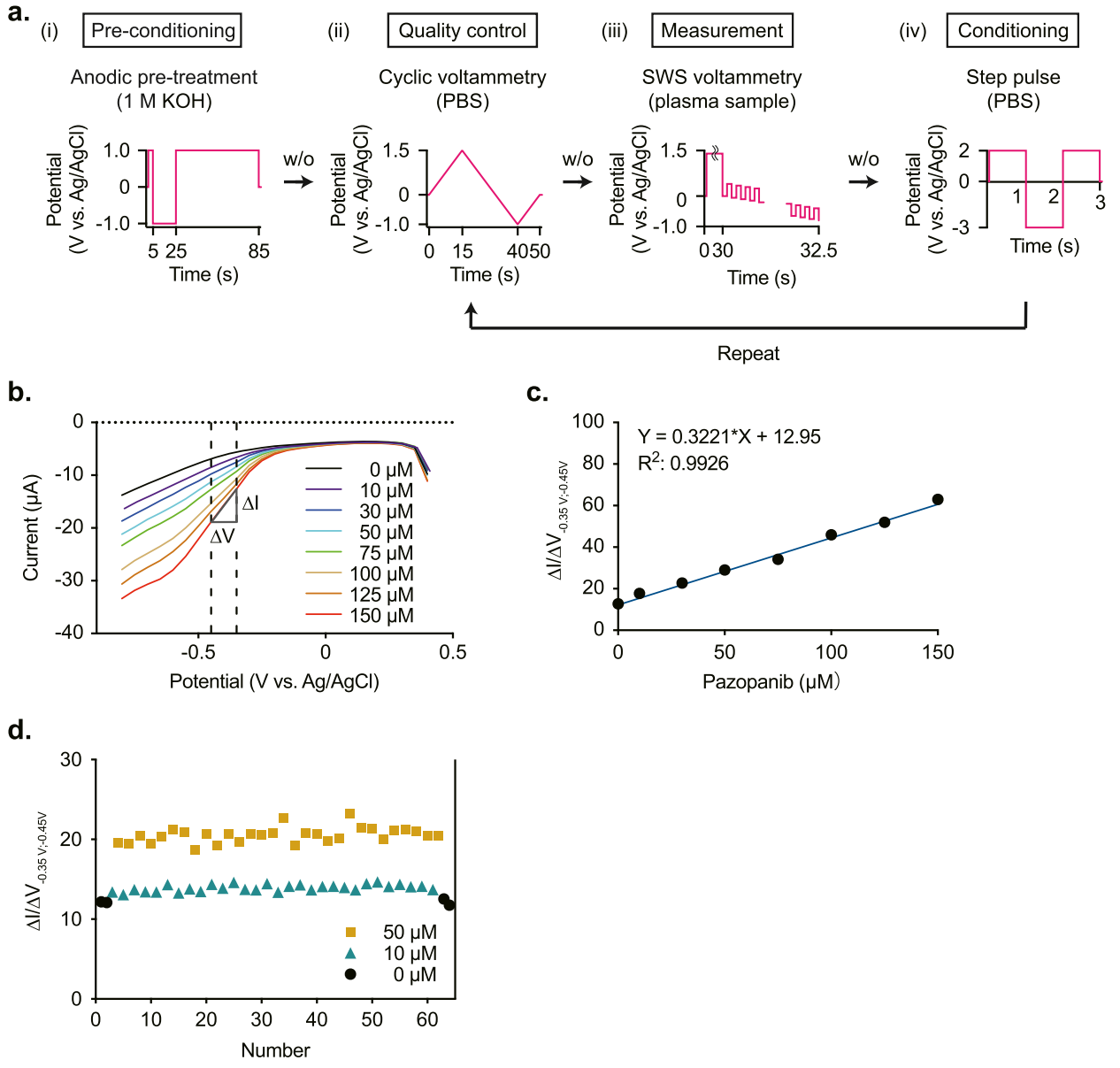

Fig. 3. Optimisation and evaluation of the detection protocol of pazopanib. *a*, The optimised potential protocol for electrochemical detection of pazopanib in rat plasma. The protocol consists of four procedures; (i) 'pre-conditioning' chronoamperometry in a 1 M KOH solution (1 mL) for electrode surface O-termination (initial potential: 0 V versus Ag/AgCl, −1.0 V for 20 s, and 1.0 V for 60 s), (ii) two cycles of cyclic voltammetry in PBS (120 μL) for 'quality control' (sweep rate: 0.1 V s^{-1}, potential window: −1.0–1.5 V, initial potential: 0 V), (iii) Square wave stripping (SWS) voltammetry for 'measurement' in a sample (120 μL) (deposition potential: 1.4 V, deposition time: 30 s, potential range: −0.8 to 0.4 V, ΔE: 50 mV, square-wave frequency: 10 Hz, pulse amplitude: 50 mV), and (iv) 'conditioning' chronoamperometry in PBS (120 μL) (initial potential: 0 V, 2.0 V for 1 s, −3.0 V for 1 s, and 2.0 V for 1 s). Before (i), (ii), and (iii), the electrode surface was washed (w/o) with ultrapure water. Procedures (ii) to (iv) were repeated for sequential multiple-time measurements. *b,* Measurements of pazopanib levels in rat plasma by SWS voltammetry. Plasma samples spiked with the drug at different concentrations (0–150 μM; *inset*) were processed by several procedures including the addition of acetonitrile as depicted in Supplementary Fig. S3b before the electrochemical detection with a boron-doped diamond (BDD) chip (chip ID: D). For each concentration, slope values obtained at the current amplitudes of −0.35 V and −0.45 V ($\Delta I/\Delta V_{-0.35\ V;-0.45\ V}$; see Figshare 1; https://doi.org/10.6084/m9.figshare.19313882) are plotted in *panel c*. *c,* The calibration curve. The slope and R^2 of the regression line are indicated. *d,* Repeatability of measurement with a BDD chip (chip ID: E). In this experiment, the sequential protocol shown in *a* was utilised, and $\Delta I/\Delta V_{-0.35\ V;-0.45\ V}$ values are plotted in the *panel*. Initially, rat plasma alone was assayed twice. Thereafter, plasma containing pazopanib at 10 or 50 μM was alternately analysed 30 times for each sample. Finally, the control plasma was again analysed twice. Consequently, 64 measurements were carried out.

Table 1
Evaluation of the repeatability of measurement with a BDD chip.

Pazopanib	$\Delta I/\Delta V_{-0.35\ V;-0.45\ V}$		
	Standard deviation	Mean	Coefficient of variation (%)
0	0.27	12.14	2.2
10 μM	0.42	13.92	3.0
50 μM	0.95	20.54	4.6

The displayed values were obtained via the analysis of the data in Fig. 3d.

for 50 μM) throughout the experiment; the coefficients of variation in the 10 and 50 μM data were 3.0% and 4.6%, respectively (Table 1), which were much less than 15%, i.e. the standard precision level for bioanalyses [10,32]. Moreover, interclass correlation coefficients ICC(1, 1) and ICC(1, 30) were 0.975 and 0.999, respectively, indicating high reliability of the repeated measurements (≥0.90) [33]. It is also noteworthy that the baseline values obtained two times with blank plasma at the outset of the assay were almost identical and closely matched those recorded at the end (the coefficient of variation: 2.2%, mean value for $\Delta I/\Delta V_{-0.35\ V;-0.45\ V}$: 12.14; Fig. 3d and Table 1).

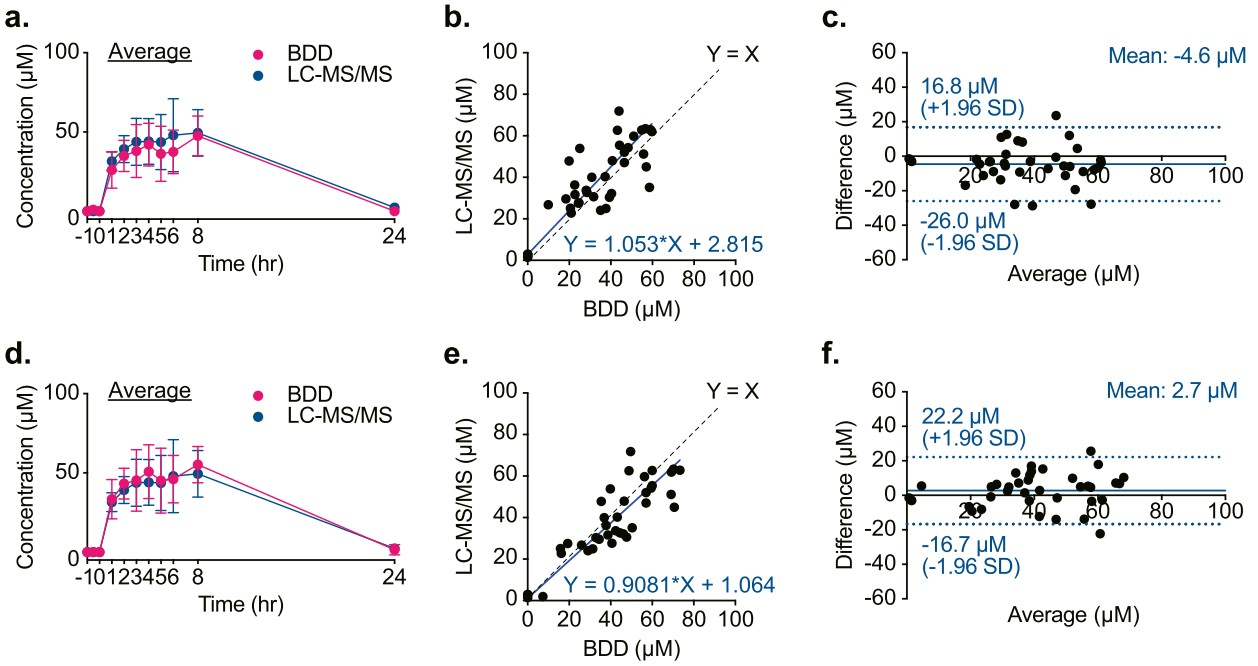

Fig. 4. Analysis of plasma from rats treated systemically with pazopanib. Five healthy rats were orally given pazopanib once at the dose of 100 mg mL^{-1} kg^{-1} (time point: zero), and then, whole blood (180 μL) was collected at time points 1, 2, 3, 4, 5, 6, 8, and 24 h. The extracted plasma samples were processed by the protocol described in Supplementary Fig. S3b and subjected not only to square wave stripping (SWS) voltammetry with a boron-doped diamond (BDD) chip (chip ID: F) in the tabletop system but also to the measurement by liquid chromatography coupled with tandem mass spectrometry (LC–MS/MS). Note that before the drug administration, blood samples were taken three times and analysed with the same method to record the baseline response. Regarding the experiments in panels *a*–*c*, for each rat, $\Delta I/\Delta V_{-0.35\ V;-0.45\ V}$ values obtained by SWS voltammetry (see Fig. 3a) were converted to the concentrations by means of an individual calibration curve (Supplementary Fig. S6a) (Method #1 in the *text*). *Panel a* describes plots of averaged values (mean ± SD, n = 5), respectively [note: for a few animals, LC–MS/MS data at certain time point (s) were lacking; see Supplementary Fig. S7 and Methods]. *Panel b* is a comparison of the electrochemical and LC–MS/MS measurements. The *solid line* represents a linear relation fitted to the data via Deming regression analysis (slope = 1.053), and the *dashed line* shows $y = x$ equivalence. *Panel c* presents Bland–Altman analysis of the difference between the electrochemical and LC–MS/MS measurements (subtraction of the former from the latter) plotted as a function of the mean of these values. The *solid grey line* indicates the bias (i.e. the mean difference, −4.6 μM), whereas the dashed lines represent the 95% confidence interval (i.e. the range of 1.96 SD: −26.0 to 16.8 μM). In *d*–*f*, the $\Delta I/\Delta V_{-0.35\ V;-0.45\ V}$ values obtained from the rat plasma collected over time are converted to analyte concentrations by a different method as follows (Method #2 in the *text*). The 'general' slope of the calibration curve was determined from the linear regression that was derived from the electrochemical data (measurements of 0–150 μM pazopanib) from all the five rats (Supplementary Fig. S6b). Then, for each rat, the average of the measurements carried out three times before the drug administration was used as baseline (i.e. 0 μM) for computing the concentrations. In *panel d*, the electrochemical measurement for the average data on the five rats is displayed and compared to the LC–MS/MS measurements. *Panels e* and *f* are a scatter plot (slope for Deming regression = 0.9081: *solid line*, $y = x$ equivalence: *dashed line*) and a Bland–Altman plot (bias: 2.7 μM, 95% confidence interval: −16.7–22.2 μM), respectively.

2.2. Examination of BDD-chip systems with the samples from dosed animals and humans

2.2.1. Analysis of plasma samples collected from rats that received pazopanib orally

From the standpoint of clinical practice, we attempted to investigate whether pazopanib in the plasma obtained from an orally treated animal model can be quantified by a BDD chip (chip ID: F; Fig. 4). In mammals, two metabolites can be derived from pazopanib, but their amounts are negligible (<5% proportion for each) [34]. Therefore, we focused on the parent compound for the analyses. From each of five healthy Wistar rats (animal IDs: Rt01−05), whole blood was initially collected three times at an interval of ~0.5 h for determining the baseline level, a calibration curve (Supplementary Fig. S6a), and the limit of detection (LOD), followed by single oral administration of the drug at 100 mg mL^{-1} kg^{-1}. After that, the blood (180 μL) was longitudinally collected at time points 1, 2, 3, 4, 5, 6, 8, and 24 h (see 'Protocol 2' in Supplementary Fig. S3b). Fig. 4a illustrates the average result for all five tested animals (animal ID: Rt01−05). In this assay, $\Delta I/\Delta V_{-0.35\ V;-0.45\ V}$ values obtained by SWS voltammetry were converted to analyte concentrations by means of the calibration curve unique to the tested rat (termed 'Method #1'). The plasma drug level abruptly went up in 1 h; it continued to increase and reached a peak of 62.6 ± 8.0 μM (mean ± SD, n = 5) at 8 h among the blood-sampling time points. At 24 h, the concentration returned to baseline. Among the five rats, time to the maximum concentration varied to some extent (Table 2 and Supplementary Fig. S7a), as reported elsewhere [35]. As an additional assessment of the quantitative nature of the pazopanib detection by the BDD chip, the plasma samples collected at different time points in all the rats were analysed by LC−MS/MS. In the average data, overall, the measurements were comparable to the data generated by the BDD chip (Fig. 4a). This similarity was observed in each case of the individual rats (animal IDs: Rt01−05, Supplementary Fig. S7a). In support of this finding, when pazopanib concentrations measured by LC−MS/MS were plotted against those determined by the BDD chip, the slope of Deming regression (i.e. errors-in-variables regression) was 1.053 (Fig. 4b). Moreover, a Bland−Altman plot indicated a small bias of −4.6 ± 10.9 μM (i.e. the mean difference between the values obtained by two methods ± SD; Fig. 4c) [36]. The majority of the data points fell within a 95% confidence interval of −26.0 to 16.8 μM, indicating that there was little systematic variation between the results obtained with the two methods. Therefore, the BDD-based system can, at least semi-quantitatively, determine plasma pazopanib concentrations.

In terms of possible practical use of the BDD chip–based system at a clinical site, it is unrealistic to build the chip's calibration curve for each patient in advance. In this regard, in a series of analyses depicted in Fig. 4d, a curve's slope was determined from the linear regression that represented the electrochemical assays (0−150 μM pazopanib) of the samples from all the five rats (Supplementary Fig. S6b). This 'general' slope likely corresponds to the average value of all the animals or even to the value obtained using other standard samples. Then, for each rat, the average of the $\Delta I/\Delta V_{-0.35\ V;-0.45\ V}$ values obtained three times before drug administration was used as a zero μM reference. The data analysed with this 'Method #2' fell into a sufficiently acceptable range for quantitativity, as compared to the data from LC–MS/MS (Fig. 4d for the average data from the five rats; see Supplementary Fig. S7b). The slope of Deming regression was 0.9081 (Fig. 4e), and bias and the 95% confidence interval in the Bland−Altman plot were 2.7 ± 9.9 μM and −16.7 to 22.2 μM, respectively (Fig. 4f).

2.2.2. Detection of pazopanib in clinical samples

We next investigated whether a BDD chip in the tabletop system can quantify plasma pazopanib in patients (Fig. 5). Eight participants (patient IDs: Pt01−08) with different sarcoma types and various clinical characteristics received the drug orally once a day; six patients took other drug(s) before or during pazopanib treatment (Fig. 5a and Figshare 2; https://doi.org/10.6084/m9.figshare.19313900.v1). In each patient, the dose of pazopanib was determined or controlled in accordance with his or her physical condition, age, symptoms of the primary disease, complications, and adverse effects induced by the drug during a period of monitoring (8 or 16 days). Note that in two patients (patient IDs: Pt06 and Pt08), pazopanib treatment was discontinued due to severe general fatigue and bradycardia, respectively. Blood samples (6 mL) were collected from individuals at four time points: ~20−2 h before and 2 h after the first drug administration and immediately before the drug administration on the 3rd and 8th days (i.e. trough values) (except for Pt06 whose final sample was taken on the 16th day). Then, the plasma fractions were processed ('Protocol 2' in Supplementary Fig. S3b), and the concentrations were determined by two approaches [1]: a BDD chip (chip ID: F) with 'Method #2', which involved the 'general' calibration curve constructed from the data on all the patients (Supplementary Fig. S8a) and the measurement of $\Delta I/\Delta V_{-0.35\ V;-0.45\ V}$ in the samples initially collected from the patients to implement the zero μM reference, and [2] LC–MS/MS. Overall, the results were consistent between the two approaches except for the data on the 8th day in Pt07 and on the 3rd day in Pt08 (Fig. 5a). A scatter plot indicated that the slope of Deming regression was 0.88 (Fig. 5b), which likely rivals the performance of commercially available sensors for C-reactive protein, glucose, or haemoglobin [37]. In the Bland−Altman plot (Fig. 5c), bias was small, 4.4 ± 13.1 μM, and most data points were within the 1.96 SD range (i.e. 95% confidence interval: −21.3–30.0 μM). These

Table 2
Pharmacokinetic parameters of pazopanib in rats.

	Rt01	Rt02	Rt03	Rt04	Rt05	Average	SD
Peak concentration ($C_{max,obs}$, μM)	73.3	60.0	69.2	50.4	60.0	62.6	8.0
Time to maximum concentration ($t_{max,obs}$, h)	8	4	3	8	5	5.6	2.1
Area under the curve (AUC_{8h}, μM·h)	469.4	311.4	345.2	210.9	375.2	342.4	84.2

$C_{max,obs}$: maximal drug concentration among the blood-sampling time points.
$t_{max,obs}$: time to $C_{max,obs}$ at blood-sampling points.
AUC_{8h}: area under the curve from zero to 8 h.

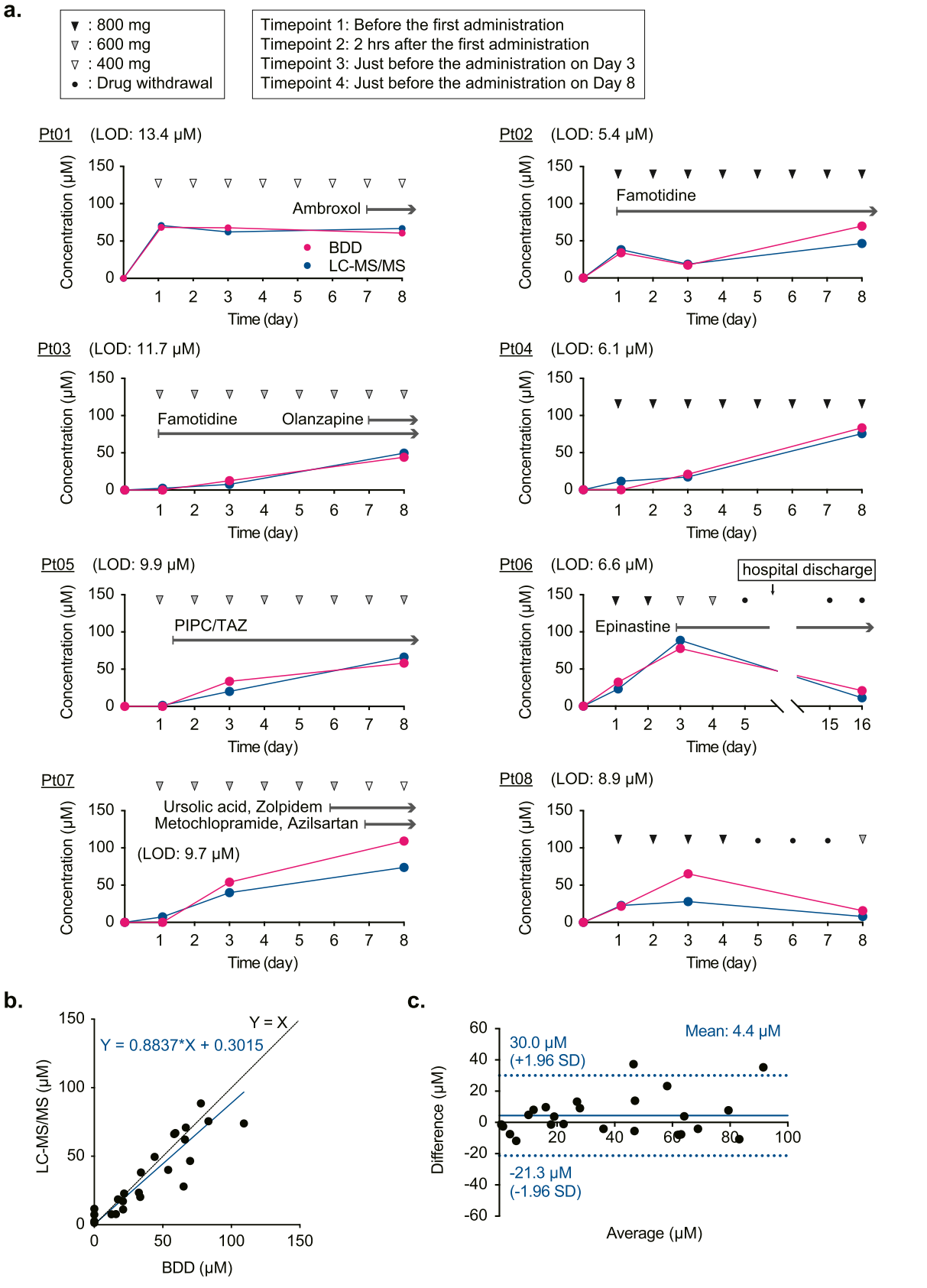

(caption on next page)

Fig. 5. Detection of pazopanib in plasma from orally treated patients. *a,* Monitoring of plasma pazopanib concentrations in individual patients. Eight participants with sarcoma were given pazopanib at 800, 600, or 400 mg basically once a day (*closed*, *grey*, and *open arrowheads*, respectively; see the *left box*) starting from Day 1. Some patients took other drug(s) before and/or during pazopanib treatment (*arrows* above the data plots and Figshare 2; https://doi.org/10.6084/m9.figshare.19313900.v1). The chemotherapy was discontinued on Day 5 in Pt06 and Pt08 (*closed circles*); the latter patient resumed the therapy on Day 8. Whole-blood samples (6 mL) were collected from each patient at four time points; ~20−2 h before and 2 h after the first pazopanib administration and immediately before the administration on the 3rd and 8th days (see the *left box*) (except for Pt06, whose final sampling was performed on Day 16). Then, in the extracted plasma fractions, the concentrations were determined by means of a BDD chip (chip ID: F) in the tabletop system with 'Method #2' (see the *text*) as analysed in Fig. 4d (see also Supplementary Fig. S3b) as well as by LC–MS/MS. The former analysis involved the 'general' calibration curve, which represented a summary profile of the calibration curves of all the patients (Supplementary Fig. S8a). Limits of detection (LODs) obtained in the electrochemical analysis are indicated in each *panel*. Note that in the Pt05 dataset, the LC–MS/MS measurement before the drug administration is missing because of a loss of the plasma sample owing to our technical error (see Methods). PIPC: piperacillin, TAZ: tazobactam. *b,* Comparison of the BDD electrochemical measurements and LC–MS/MS analyses. The *solid line* indicates the regression line of Deming's method (slope = 0.8837), and the *dashed line* shows $y = x$ equivalence. *c,* The Bland–Altman plot assessing the difference between the two methods. Bias (*grey line*) is 4.4 μM, and the 95% confidence interval (*doted lines*) is −21.3 to 30.0 μM.

observations confirmed the accuracy of the measurements by means of the BDD chip system.

2.3. Evaluation and modification of BDD-chip systems for possible clinical applications

2.3.1. Repeatability and reproducibility of the measurement with BDD electrodes

As depicted in Fig. 6, we evaluated BDD's performance in multiple ways. First, each of the two chips tested in Fig. 3 (chip IDs: D and E) was again subjected to SWS voltammetry (see Fig. 3a), with 0–150 μM pazopanib dissolved in plasma collected from multiple rats (animal IDs: Rt06−17), and the calibration curves' slope values were compared to those generated by chip F for the assays of the orally treated rats (see Fig. 4). Mean ± SD values were 0.35 ± 0.04 for chip D (n = 6; Supplementary Fig. S9a), 0.15 ± 0.01 for chip E (n = 6; Supplementary Fig. S9b), and 0.26 ± 0.04 for chip F (n = 5; Supplementary Fig. S6a). For each individual chip, the slope values were similar, as confirmed by the coefficient of variation of approximately ≤~15% (Table 3) [10,32]. With chip F, when spiked plasma samples of five different guinea pigs were tested (animal IDs: GP01−05, Supplementary Fig. S10), the result was 0.27 ± 0.01 (mean ± SD), which resembled the aforementioned rat data and even the results on patients' plasma (0.30 ± 0.01; n = 8; Supplementary Fig. S8b; $p = 0.8889$ and 0.063, respectively, one-way ANOVA and *post hoc* Tukey's test). These observations confirmed remarkably high repeatability of the measurement (see Fig. 3d). Nonetheless, significant sensor-to-sensor variability of the slope was observed among the three chips (rat samples; $p < 0.0001$ for chip D versus chip E and chip E versus chip F; $p < 0.001$ for chip D versus chip F;

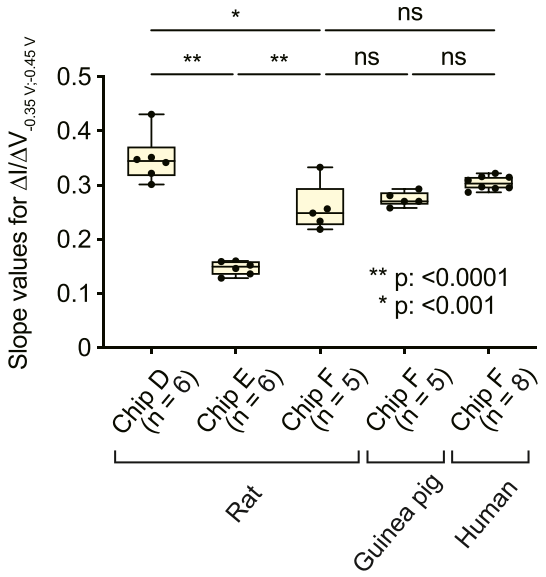

Fig. 6. Assessment of the repeatability and reproducibility of the measurements with BDD chips. In this series of analyses, three different chips (chip IDs: D, E, and F) set in the tabletop system were tested with pazopanib (0–150 μM; see the *inset* in Fig. 3b) dissolved in plasma collected from individual rats, guinea pigs, or patients with sarcoma; the protocol for the measurements was identical to the one described in Fig. 3a. Then, the $\Delta I/\Delta V_{-0.35\ V;-0.45\ V}$ slope values of the calibration curves were determined as depicted in Fig. 3c, and these values are indicated in *box-and-whisker plots*: the *boxes* show a median and the 25th to 75th percentiles, whereas the *whiskers* represent the lowest and highest value in the range between the 25th percentile minus 1.5 interquartile ranges and the 75th percentile plus 1.5 interquartile ranges, respectively. The number of the animals and humans analysed with each chip is given underneath the *bars*. *Asterisk(s)* indicate a significant difference from the rat data of chip F (*$p < 0.001$, **$p < 0.0001$, Tukey's multiple-comparison test after one-way ANOVA; ns, not significant). Raw data of the calibration curves analysed for this *panel* are shown in Supplementary Fig. S6a, 8b, 9, and 10.

Table 3
Evaluation of each BDD chip's slope.

	$\Delta I/\Delta V_{-0.35\ V;-0.45\ V}$			
	Standard deviation	Mean	Coefficient of variation (%)	Limit of detection (μM)
Chip D (rat)	0.04	0.35	11.6	2.73
Chip E (rat)	0.01	0.15	7.4	5.96
Chip F (rat)	0.04	0.26	15.3	7.40
Chip F (guinea pig)	0.01	0.27	4.2	2.91
Chip F (human)	0.01	0.30	3.8	8.41

The displayed values were obtained by the analysis of the data in Fig. 6.

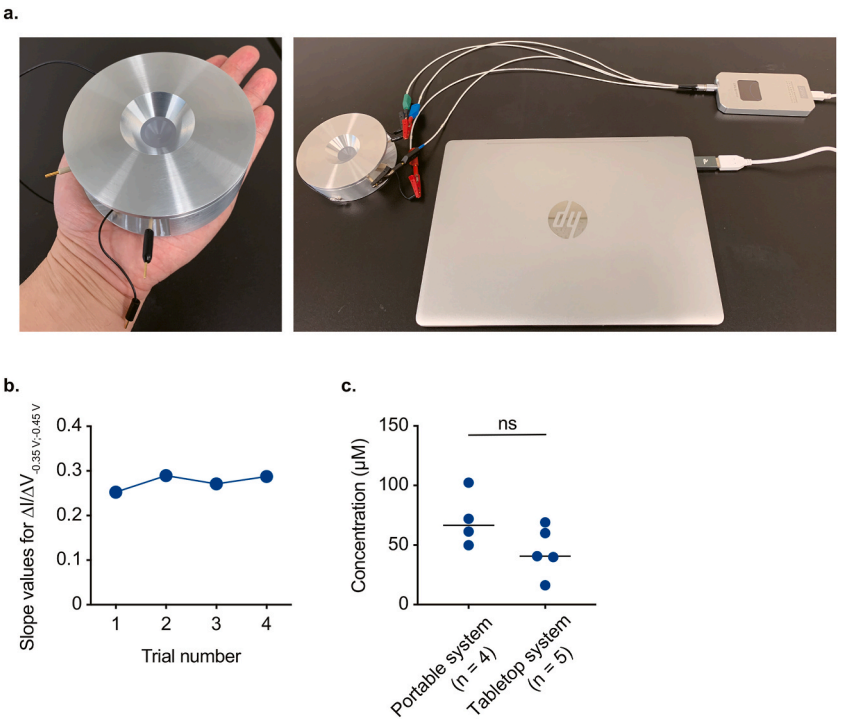

Fig. 7. Fabrication and evaluation of a prototype of the portable drug-monitoring system. *a,* The measurement setup. The system is made up of a handheld disk-shaped device containing a boron-doped diamond (BDD) chip (*left panel*, see Supplementary Fig. S11), a smartphone-shaped potentiostat, and a laptop computer (*right panel*). *b,* Repeatability of the measurement. By means of the portable system (chip ID: H), a calibration curve was obtained four times using rat plasma spiked with different amounts of pazopanib (0–100 μM; Supplementary Fig. S12a; for the protocol, see Fig. 3a–c), and the $\Delta I/\Delta V_{-0.35\ V;-0.45\ V}$ slope values are plotted in the *panel*. *c,* Evaluation of the data from the portable system. In this series of experiments, four healthy rats were given pazopanib orally once at the dose of 100 mg mL^{-1} kg^{-1}. From each rat, ~40 μL of whole blood was collected immediately before and 5 h after the drug administration, and the plasma samples were analysed with the portable system (chip ID: I; for protocols, see Fig. 3a–c and Supplementary Fig. S12b). The $\Delta I/\Delta V_{-0.35\ V;-0.45\ V}$ values obtained in the 5 h samples were converted to the concentrations via the calibration curve (Supplementary Fig. S12c), which was constructed in advance using commercially available rat plasma spiked with different amounts of pazopanib (0–100 μM) (Method #2 in the *text*). In this calculation, the $\Delta I/\Delta V_{-0.35\ V;-0.45\ V}$ values before the drug administration served as baseline (i.e. 0 μM). In the *panel*, the concentrations are compared to the 5 h data obtained by the tabletop system (see Fig. 4d and Supplementary Fig. S7b); $p = 0.11$, according to the Mann–Whitney *U* test; ns: not significant.

one-way ANOVA and *post hoc* Tukey's test).

2.3.2. *Fabrication and testing of a portable system for TDM*

Again, the amounts of whole blood collected from rats and patients dosed with pazopanib were 180 μL and 6 mL, respectively (Figs. 4 and 5). Nevertheless, considering the sample volume (120 μL) applied to the BDD chip for electrochemical detection of the drug in the tabletop system, the minimal required volume of whole blood was estimated to be ~60 μL. In spite of such small volume of the sample, setting up the tabletop system requires considerable space: 1.5 × 1.5 m^2 (Supplementary Fig. S1). Therefore, to make the system smaller and reduce the invasiveness of blood sampling, we fabricated a prototype of a portable system, which harbours a handheld disk-shaped biosensor 10 cm in diameter and 3.4 cm thick (Fig. 7a). This device contains a tiny cylindrical chamber, which houses a BDD chip at the bottom (reaction area: 9.6 mm^2, applied sample volume: 60 μL; Supplementary Fig. S11). In addition, we

included a smartphone-shaped potentiostat (pocketSTAT: 115 × 59 × 13 mm; Ivium Technologies B•V.), and a laptop computer for the convenience of measurement (Fig. 7a). The accuracy of the applied potential and the measured current of this potentiostat is basically similar to that of the potentiostat in the tabletop system (see Methods). Using this system (chip ID: H), a calibration curve was built four times by means of rat plasma spiked with different concentrations of pazopanib (0–100 μM) (animal ID: Rt18; Supplementary Fig. S12a). $\Delta I/\Delta V_{-0.35\ V;-0.45\ V}$ slope values were relatively stable, 0.25 to 0.29, confirming the high repeatability of the measurement (Fig. 7b). Next, to mimic clinical practice, ~40 μL of blood was collected from each of four rats (animal IDs: Rt19–22) immediately before oral administration of pazopanib (100 mg mL^{-1} kg^{-1}) and 5 h after the drug administration. Then, the plasma samples were processed by basically the same method as the one applied to clinical samples ('Protocol 3' in Supplementary Fig. S12b), and the resultant samples were analysed electrochemically (chip ID: I). The concentrations at 5 h were converted by aforementioned 'Method 2' via the calibration curve obtained with commercially available rat plasma (Supplementary Fig. S12c). These values were similar to the 5 h values determined in animal experiments with the tabletop system, as presented in Fig. 4d ($p = 0.11$, Mann–Whitney U test; Fig. 7c). Notably, the sampling-to-result time of this portable system never exceeded 10 min.

3. Discussion

In this work, we demonstrated that the electrochemical method based on engineeringly unmodified BDD chips semi-quantitatively and selectively determines 'total' plasma concentration of pazopanib within its therapeutic range (Figs. 1, 2, and 3a–c). Notably, these useful characteristics were documented in the analyses of animal and clinical samples (Figs. 4 and 5) –it can be emphasised that patient plasma samples were assayed by means of a BDD electrode for the first time. The BDD chip manifested high repeatability of the

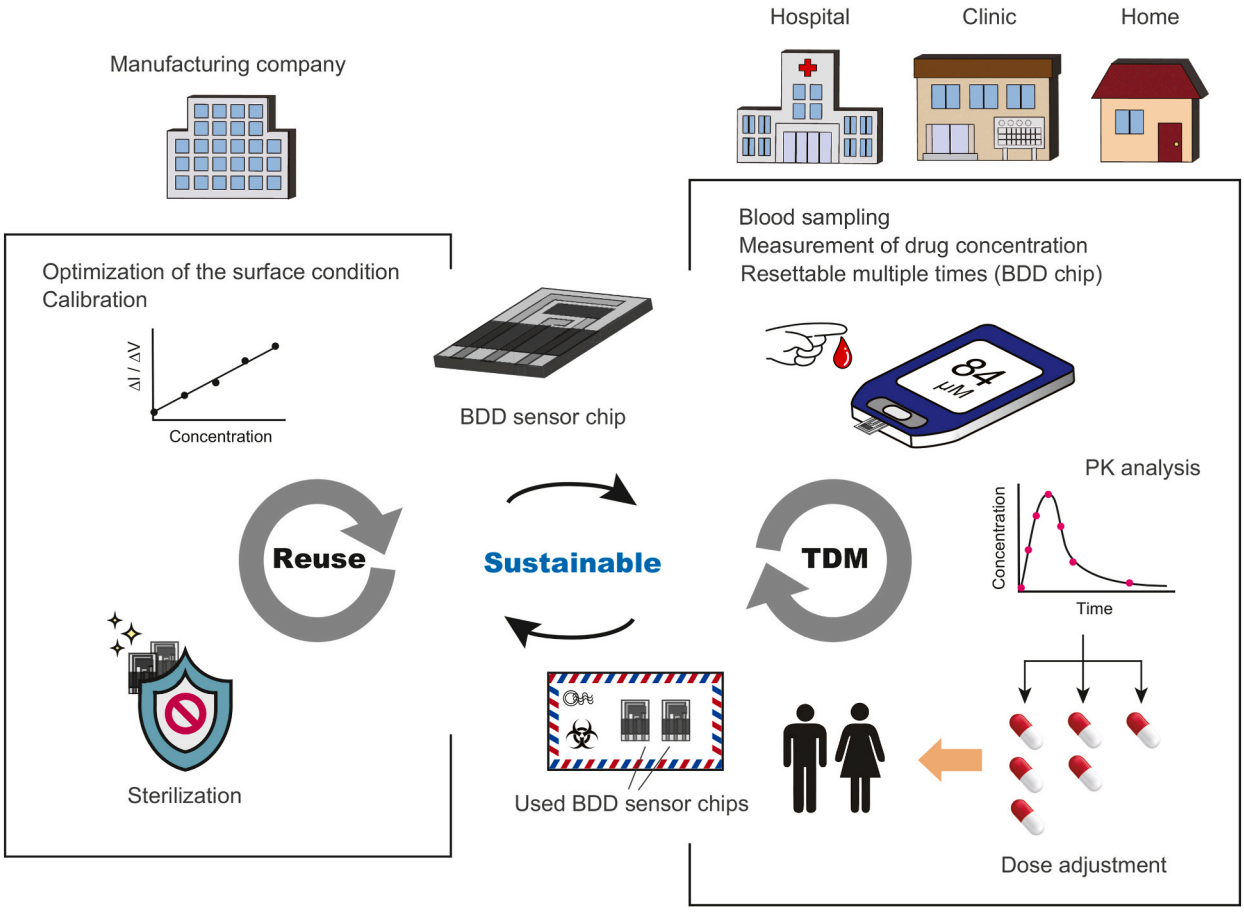

Fig. 8. Prospects for therapeutic drug monitoring (TDM) with boron-doped diamond (BDD) chips. Schematic illustration in the *right box* shows expected TDM with BDD chips in the future. A mobile handheld all-in-one biosensor based on a BDD chip measures drug concentration in a few droplets of whole blood with short sampling-to-result time: several seconds to a few minutes. The chip can be semi-automatically reset multiple times with a washing kit and potential protocols for the conditioning and quality control (see Fig. 3a). The pharmacokinetic data obtained frequently over time are gathered on site in hospitals or clinics or online from patients' homes, are analysed by medical or pharmacological experts or even by artificial intelligence, and are used for personalised control of medication dosage in patients. The BDD chips are transported to the manufacturer, processed via a few simple steps described in the *left box*, and then reused. This strategy with sustainable BDD chips is environmentally friendly and may reduce medical costs.

measurement and therefore is sustainable (Figs. 3d and 6). The portable system with the handheld biodevice containing the chip determined the drug concentration in a small sample (~40 μL) of whole blood with short turnaround time (~10 min; Fig. 7). This less invasive and speedy method with the possibly reusable sensor represents a low-cost strategy that can contribute to advances in TDM and may improve medication adherence.

3.1. Advantages of drug-monitoring systems based on BDD

The key factors for the development and dissemination of convenient drug detection systems are accuracy, precision, low cost, and simplicity. The quantitativity test of the BDD chips with clinical samples revealed that total imprecision relative to LC−MS/MS is ~12% (slope of Deming regression is 0.88; Fig. 5b). This value is comparable to accuracy criteria for glucose meters (12−20%) and to the discrepancy between well-established immunoassays and reference methods (12−15%) [36,38,39]. A limited number of recently created portable biosensors based on an immunoassay, surface plasmon resonance, or electrochemistry were evaluated in terms of quantitativity by means of clinical blood samples [5,11–14]. These systems require an antibody or enzyme that selectively recognises a given drug with high sensitivity, and the difficulty with finding such bioreceptors is likely a critical problem. As for the sensor involving an enzyme and aptamer, additional technologies are necessary that immobilise such drug-recognizing components without a loss of their function on the surface of materials having specific physicochemical properties. In contrast, without such time-consuming and costly procedures, our system shows excellent selectivity, as validated on clinical samples containing various drugs and biological substances (Fig. 5). This advantage is based on the properties of the native BDD electrode: theoretically, with simple optimisation of the potential protocol, this electrode can detect a wide variety of drugs. Indeed, we found that voltammetry with different protocols in the tabletop system (chip ID: J) successfully detected another molecular-targeting anticancer drug, lenvatinib, and an anthracycline cytotoxic agent, doxorubicin, within their therapeutic concentration ranges (0.10−0.21 μM for lenvatinib, 10−100 nM for doxorubicin; Supplementary Fig. S13) [40,41]. Note that, although the potential that induced a peak current in reduction reaction with lenvatinib resembled the case of pazopanib, these two drugs, which share similar mechanisms of action, are not administered to the patients simultaneously in clinical practice. Our electrochemical approach may also be applicable to certain classes of antibiotics, antimalarial drugs, antiepileptic drugs, antidepressants, other anticancer drugs, and vitamins, all of which have been detected by cyclic voltammetry with a BDD electrode in our earlier works [42,43]. Among some of the drugs, the potential that can induce redox current (s) is different. This property may allow us to separately measure the concentrations of different compounds at their unique potentials in the plasma sample from a patient treated with multiple drug therapy. The inexpensiveness of our strategy is further proven as follows. As shown in Figs. 3d and 6, a BDD chip can be repeatedly used ≥60 times via a simple reset procedure (i.e. washing with water followed by electrical treatment; Fig. 3a). The excellent repeatability enables the reuse of the chip as the sensing element, thus reducing the cost of drug monitoring. This benefit may still be present even if the BDD chip serves as a disposable sensor: the fabrication price of the chip is estimated to be less than ~ US$5. Moreover, the palm-sized device, the exchangeable chip, potentiostat, and data analysis platform can be integrated together into a handheld all-in-one instrument that may be produced at a low cost just as common portable glucose meters (~US$50), which are based on similar detection machineries, and comparably to a recently developed universal mobile electrochemical detector (~US$25) [44]. The BDD-based all-in-one device, which can facilitate on-site drug detection, may improve pharmacotherapy outcomes not only in developed but also in developing countries.

Another noteworthy advantage of our approach is measurement rapidity. The portable system permitted us to determine plasma drug concentrations within a short sampling-to-result time of ~10 min (Fig. 7 and Methods). To our knowledge, this performance is better than the turnaround time of other recent point-of-care biosensors (15−90 min) [45,46]. Additional merits of the operating procedures are outlined below. Measurement accuracy was verified by means of rat and patient samples and a 'general' calibration curve (Fig. 4–f and 5). This observation indicates that before shipping to clinical sites, BDD chips can be calibrated with any standard plasma samples, even commercially available products (see Fig. 7c). The portable system requires ~40 μL of whole blood for the drug quantification. Such small volume can be easily collected with low invasiveness by a finger prick and a capillary-type disposable microtube, which can be operated even by non-healthcare workers. All the procedures for the sample preparation and assay in our current method can be carried out via simple pipetting and centrifuging; although these tasks may be less convenient, they do not require well-trained personnel. In this regard, our portable system, even in its current form, may be useable in laboratories of medium-size and small hospitals and clinics. This application should become more realistic when the assay system is equipped with handy machinery that promptly removes the cells and proteins from a whole-blood sample without the manual procedures and is accompanied by a cleaning kit and potential protocol that semi-automatically wash and reset the BDD chip on site.

Given that these improvements and the development of the aforementioned all-in-one mobile device will be achieved in the near future, we propose a point-of-testing system with the reuse of BDD chips for TDM not only at a local pharmacy but also in patients' homes (Fig. 8). This strategy along with the 'green' electrochemical material may reduce the pollution caused by disposable devices and thereby may fit the 'sustainable development goals' adopted by the United Nations in 2015 (https://sdgs.un.org/goals).

3.2. Limitations of systems with BDD chips

Despite the remarkable advantages of the method based on BDD chips, this approach has a few limitations. First, the number of the drug types that are electrochemically detectable is restricted, although this and our earlier works showed that 12 compounds are active on BDD electrodes [42,47]. The second issue is related to the specificity of drug detection. In patients who take many pharmaceuticals or have an unstable physical condition, the redox current evoked by the target drug may overlap with the responses induced by other compounds or their metabolites. This interference may explain the observation that in two data points of our experiments with clinical

samples, the BDD measurement results exceeded the LC−MS/MS measurement results by 1.5−2-fold (Fig. 5a). In addition, quantitatively fluctuating endogenous biological substances may impair or apparently enhance the response of the drug. This possibility may underlie the inconsistency between the BDD and LC−MS/MS data not only in human samples (Fig. 5) but also in rat samples (Fig. 4). The cross-redox reactivity at target potential(s) should be more carefully considered for clinical applications of such BDD systems. Third, for drug quantification, a BDD electrode is likely to be less sensitive than conventional methods such as LC−MS/MS. In this regard, the therapeutic range of some drugs will be undetectable with our approach. To address these shortcomings, the potential protocol, the data analysis method, and the amounts or types of the organic solvent, supporting electrolyte, and surfactant can be optimised. Finally, although all the chips tested in this study were derived from the same BDD wafer plate, sensor-to-sensor reproducibility of the data were variable to some extent (Fig. 6). Therefore, in the current situation, calibration curve must be obtained for each chip. Resolving this issue by developing the technique that can deposit BDD more uniformly and stably throughout the silicon wafer surface is a key step for the device's mass production for introduction into the clinic.

3.3. Prospects of TDM in oncology

There is no doubt that the use of molecular-targeting drugs will be extended to more cancer types. Accordingly, we selected pazopanib in this study. In most studies directed to TDM for pazopanib, the compound is detected by LC−MS/MS [48,49]. This conventional approach requires expensive instruments and well-trained personnel (see 'Introduction'). For electrochemical analysis, Bilge et al. used a glassy carbon electrode modified with CuO nanoparticles [50]. Using human serum 'spiked' with pazopanib, they achieved a linear calibration from 0.2 nM to 1.0 μM by means of square wave voltammetry. Nevertheless, this range is far less than the therapeutic window (43.3−97.1 μM) [31], which was successfully detected in this study (Fig. 3b and c). Our analysis with clinical samples highlighted individual differences in pharmacokinetics among the eight patients (Fig. 5a). This finding reinforces the idea that for molecular-targeting reagents, TDM is valuable [21,51]. Nevertheless, this approach is still uncommon in clinical practice, likely because growing scientific evidence is not yet sufficient to clearly prove the efficacy of dose modification for individual patients. In this context, clinical pharmacokinetic studies accompanied by an evaluation of patient outcomes (by pharmacodynamic assays, with collation of their results with the pharmacokinetic data) as well as randomised clinical trials designed to assess the effect of TDM are insufficient [2,52]; however, a possible problem is that only a limited number of institutions have and can handle expensive and labour-intensive LC−MS/MS equipment. Indeed, the initial capital cost of this conventional method is roughly estimated to range from $30,000 to $65,000 [53]. Large-scale prospective studies may become more accessible by means of the simple low-cost strategy involving the portable BDD biosensors, which are likely to have lower operating costs compared to LC−MS/MS.

Additionally, a few studies investigate the economic impact of TDM from a different perspective [54,55]. In the case of imatinib, the TDM intervention likely incurs an incremental cost-effective ratio of −$109,184 to $76,027 per quality-adjusted life years (QALY), which is below a typical willing-to-pay threshold of ~$100,000 per QALY. The TDM intervention for pazopanib with the low-cost BDD biosensors will likely have an even greater impact; the price of fabrication of the chip is estimated to be less than ~ US$5 (see above), which could significantly reduce the cost for measurement by >90% as compared to that of LC−MS/MS (~US$80) [54].

3.4. Processes of redox reaction in pazopanib

Compounds that possess nitro group, amino group, carboxy group, and/or quinones are prone to be electrochemically active [56]. As shown in Fig. 1a and Supplementary Fig. S2a, cyclic voltammetry with pazopanib indicated not only an anodic current but also a cathodic current. The oxidation response is likely induced by the formation of a hydroxylated product from an amine group found in the aminobenzenesulfonamide moiety of the compound [50,57]. This product can be further oxidized into quinones, which can be subsequently reduced at negative potentials [56,58]. Several other tyrosine kinase inhibitors possess an aminobenzene structure; indeed, imatinib and axitinib are both electrochemically detectable [59,60]. Therefore, this anti-cancer drug type can be a target for measurements using the approach described in this study.

In terms of optimisation of the procedure for the detection of pazopanib concentrations with SWS voltammetry, we selected $\Delta I/\Delta V_{-0.35\ V;-0.45\ V}$ (Fig. 3). In cyclic voltammetry (Fig. 1a), the reduction process began in a potential range between −0.45 and −0.35 V. Because at such potential window the slope of the cathodic current was likely to be the largest, the $\Delta I/\Delta V$ value in the SWS voltammogram would be maximised. More negative potentials should also induce the reduction reaction; nevertheless, at the potentials near −1 V, the current produced by other substances, including dissolved oxygen, may interfere with the current from pazopanib, as observed in the case of doxorubicin [58]. Moreover, we tested numerous combinations of the potentials with SWS voltammetry and found that the data at −0.35 V and −0.45 V ($\Delta I/\Delta V_{-0.35\ V;-0.45\ V}$) generated a sensitive and stable calibration curve (Figshare 1, https://doi.org/10.6084/m9.figshare.19313882). This potential range, which initiates the reduction reaction of pazopanib, seems to be unique to the drug, as similarly observed in other compounds that are also characterised by unique potentials inducing redox reactions. It is possible that the potential range optimised in this study may not be applicable to other experimental setups; nevertheless, on the basis of the drug's profile described above, a similar potential range would also produce a similar response in SWS voltammetry.

3.5. Pharmacokinetics of pazopanib

When the plasma from rats orally administered with pazopanib was analysed by means of BDD chips (Fig. 4 and Supplementary Fig. S7), C_{max} and t_{max} among the blood-sampling points of our protocol were 62.6 ± 8.0 μM and 5.6 ± 2.1 h, respectively (mean ± SD,

n = 5; also see Table 2). This t_{max} value is significantly longer than that obtained in another study that administered the same dose of pazopanib to rats (100 mg mL^{-1} kg^{-1}) ([61]; Supplementary Table S2), although C_{max} values are similar between the two studies. This inconsistency may be due to variations in drug absorption efficacy through intestinal epithelium, which can be affected by animal housing conditions such as the diet contents. Further studies are needed to identify the factor(s) that affect the pharmacokinetic parameters of pazopanib.

4. Concluding remarks

This work demonstrated the accuracy and reuse potential of BDD chips as a drug monitoring sensor through the analysis of plasma samples collected from animals and patients orally administered with pazopanib for the first time. Because the measurement with the BDD systems is rapid and inexpensive, this approach may accelerate the pharmacokinetics studies and provide the evidence for the effectiveness of TDM in oncology. Development of more compact and easily-handled portable systems with BDD chips could allow patients to monitor their own plasma drug concentrations at home, promoting the adoption of high-quality personalised therapies and telemedicine.

5. Methods

5.1. Fabrication of BDD electrodes

A plate-type BDD electrode used in this study was prepared with the method principally the same as that used in our earlier works [62,63]. Polycrystalline BDD films were deposited on a circular silicon wafer plate (diameter: 5 cm, thickness: 750 μm) in a microwave plasma-assisted chemical vapor deposition system (Cornes Technologies, Tokyo, Japan). By means of acetone and trimethoxyborane that were mixed at a boron/carbon ratio of 1% (i.e. 10,000 ppm boron), the plate material was charged with plasma power at 5000 W for 4 h. Quality control of the BDD was carried out by Raman spectroscopy (Renishaw System 2000; Renishaw PLC, Gloucestershire, UK) in accordance with the criteria described previously [42] (Supplementary Fig. S14). The fabricated plate electrode was divided into multiple square pieces (~1 × ~1 cm). Each of these BDD chips (chip IDs: A–J) was set in the measurement chamber of the tabletop drug detection system (Supplementary Fig. S1) or in the handheld disk-shaped device of the portable system (Fig. 7a and Supplementary Fig. S11).

5.2. Chemicals and solutions

Pazopanib (LC laboratories, Woburn, MA, USA) was dissolved in dimethyl sulphoxide (DMSO; FUJIFILM Wako Pure Chemical Corporation, Tokyo, Japan) to prepare 2, 6, 10, 15, 20, 25, and 30 mM stock solutions. Requisite volume of the stock solutions was added to PBS (FUJIFILM Wako Pure Chemical Corporation) or to plasma collected from rats, guinea pigs, or patients, and these samples were analysed electrochemically. As for lenvatinib, this compound (Cayman Chemical, Ann Arbor, Michigan, USA) was dissolved in DMSO to prepare 0.1, 0.3, 1.0, and 3.0 mM stock solutions. SDS (FUJIFILM Wako Pure Chemical Corporation) and TMA (Tokyo Chemical Industry Co., Ltd., Tokyo, Japan) were separately dissolved in ultrapure water (Thermo Fisher Scientific, Waltham, MA, USA) to prepare stock solutions at 1 M and 10 mM, respectively. All the stock solutions were stored at −30 °C until use.

The pazopanib solution administered to rats was prepared immediately before every experiment. First, requisite volume of Tween 80 (Sigma-Aldrich; St. Louis, MO, USA) was added to a 0.5% hydroxypropylmethylcellulose solution (FUJIFILM Wako Pure Chemical Corporation) to obtain 0.1% concentration of the detergent. Then, the drug was dissolved in this solution at the concentration of 100 mg mL^{-1} [64,65], and this solution was given orally to the animals at the dose of 100 mL kg^{-1} body weight. In the analysis of clinical samples, patients received pazopanib tablets (Novartis Japan, Tokyo, Japan).

5.3. Electrochemical measurements in the tabletop system

Electrochemical measurements were carried out by means of the tabletop system or the portable system. This section is focused on the experimental procedure for the former system, whose overview is illustrated in Supplementary Fig. S1. In this system, a plate-type electrode chip composed of BDD, glassy carbon (ALS Co., Ltd., Tokyo, Japan), or platinum (Sanwakinzoku, Saitama, Japan) served as the working electrode. Before installation into the system, the carbon and platinum electrodes were polished with a 0.05 μm alumina suspension, and in addition, all the electrodes including BDD chips were washed with ultrapure water. After that, each electrode chip was overlaid with a cylindrical Teflon chamber (internal diameter: 15 mm, external diameter: 21 mm, height: 15 mm, and volume: 2.3 mL). Because the chamber has a hole of a 6 mm diameter at the bottom, the electrochemically reactive surface area of the electrode was ~28 mm^2. The chamber also housed a reference electrode, which was composed of Ag/AgCl with saturated KCl (2 mm in diameter, LF-2: Innovative Instruments, Inc., FL, USA) and a counter electrode, which was made by coiling a platinum wire 0.5 mm in diameter so that the final diameter of the coil was ~2 mm and length ~3 mm. A brass plate underlaid the working-electrode chip for connection to a potentiostat (HZ-7000; Hokuto Denko, Tokyo, Japan). The device was placed in a Faraday cage, and the voltammetry and recording were performed at room temperature (25 °C).

Before the experiments with the tabletop system as presented in Fig. 1 and Supplementary Fig. S2a and 4, the surface of each working-electrode chip (i.e. the BDD, glassy carbon, and platinum chip) was first cleaned and then conditioned in PBS via two cycles of cyclic voltammetry (sweep rate: 0.1 V s^{-1}, potential window: −1.0 to 1.5 V, initial potential: 0 V versus Ag/AgCl). In other series of

electrochemical assays, at the outset of each experiment, the BDD chip was pre-treated to configure the surface state by either one of the following chronoamperometry protocols [1]: the O-termination: initial potential 0 V, stepping to 1.0 V for 5 s, stepping to −1.0 V for 20 s, and holding at 1.0 V for 60 s in 1 M KOH or [2] the H-termination: initial potential 0 V, stepping to 1.0 V for 5 s, and holding at −1.0 V for 80 s in 0.5 M H_2SO_4.

Cyclic voltammetry for basic characterisation of pazopanib dissolved in PBS was carried out at a sweep rate of 0.1 V s^{-1} with a potential window of −1.0 to 1.5 V and an initial potential of 0 V (versus Ag/AgCl; Supplementary Fig. S2). Of note, to determine pazopanib's redox state that can evoke a cathodic current, the applied potential was scanned in the positive direction from 0 to 1.5 V for oxidation of the compound and then shifted to −1.0 V; alternatively, the potential was swept in the negative direction from 0 to −1.0 V for reduction of the compound and then shifted to 1.5 V. The latter protocol was applied only in the experiment depicted in the right-hand panel of Supplementary Fig. S2a.

To detect pazopanib in plasma (for details of the preparation of plasma samples, see '*Preparation of samples from rat and guinea pig plasma*' below), the BDD chips underwent the potential protocol composed of four procedures as follows (Fig. 3a): (i) 'pre-conditioning' chronoamperometry in 1 M KOH (1 mL) for the electrode surface O-termination (initial potential: 0 V, −1.0 V for 20 s, and 1.0 V for 60 s), (ii) two cycles of cyclic voltammetry in PBS alone (120 μL) for 'quality control' (sweep rate: 0.1 V s^{-1}, potential window: −1.0–1.5 V, initial potential: 0 V), (iii) SWS voltammetry for the 'measurement' in a plasma sample (120 μL) by the optimised potential protocol (deposition potential: 1.4 V, deposition time: 30 s, potential range: −0.8 to 0.4 V, ΔE: 50 mV, square-wave frequency: 10 Hz, pulse amplitude: 50 mV), and (iv) 'conditioning' chronoamperometry in PBS (120 μL) (initial potential: 0 V, 2.0 V for 1 s, −3.0 V for 1 s, and 2.0 V for 3 s). Note that procedures (ii) to (iv) were repeated for sequential multiple-time measurements.

The samples containing lenvatinib were analysed in the tabletop system as follows. Necessary volume of the stock solution was mixed with PBS to prepare the test samples (10 μM lenvatinib). Cyclic voltammetry was carried out at a sweep rate of 0.1 V s^{-1} with a potential window of −1.0 to 1.5 V and an initial potential of 0 V (versus Ag/AgCl; Supplementary Fig. S13a). To detect lenvatinib in rat plasma (for details of the preparation of plasma samples, see '*Preparation of samples from rat and guinea pig plasma*' below), a BDD chip was subjected to the protocol similar to the one for pazopanib, with a few modifications (Supplementary Fig. S13b): (i) 'pre-conditioning' chronoamperometry in 1 M H_2SO_4 (1 mL) for the electrode surface H-termination (initial potential: 0 V, −1.0 V for 50 s), (ii) two cycles of cyclic voltammetry in PBS alone (120 μL) for 'quality control' (sweep rate: 0.1 V s^{-1}, potential window: −1.0–1.5 V, initial potential: 0 V), (iii) SWS voltammetry for 'measurement' in a plasma sample (120 μL) by the optimised potential protocol (deposition potential: 1.2 V, deposition time: 30 s, potential range: −0.8 to 0.4 V, ΔE: 50 mV, square-wave frequency: 20 Hz, pulse amplitude: 125 mV), and (iv) 'conditioning' chronoamperometry in PBS (120 μL) (initial potential: 0 V, 3.0 V for 2 s, and −3.0 V for 3 s).

5.4. Preparation of samples from rat and Guinea pig plasma containing pazopanib

Animal experiments were carried out in compliance with the protocol approved by the Institutional Animal Care and Use Committee and by the President of Niigata University (Permission Number: Niigata Univ. Res. SA00757 and SA00764) and the ethical approval from the Animal Experiment Committee of Osaka University Graduate School of Medicine (decision No. 03-062-00). The experiments were designed according to the Japanese Animal Protection and Management Law. Male Wistar rats (200–400 g, 6–40 weeks of age; SLC Inc., Hamamatsu, Japan), which are known for gender differences in drug metabolism [66], and male and female Hartley albino guinea pigs (750–1100 g, 10–40 weeks of age; SLC Inc.) were housed at the animal facilities of Niigata University or Osaka University and kept on a 12-h light/12-h dark cycle. Water and feed were available *ad libitum*. Animal handling and reporting are in compliance with the ARRIVE guidelines [67]. In total, 28 rats and five guinea pigs were used in this study; from each animal, requisite volume of whole blood was collected, and plasma was isolated as described below. The plasma samples were subjected to the following four different assays.

The first series of experiments was intended for the characterisation of the basic electrochemical profile of pazopanib in rat plasma by means of the tabletop system (Fig. 2). A rat (animal ID: Rt27) was anaesthetised deeply by an intra-peritoneal injection of 64.8 mg kg^{-1} pentobarbital sodium (Kyoritsu Seiyaku Corporation, Tokyo, Japan). A 27-gauge needle attached to a blood collection tube (Terumo Corporation, Tokyo, Japan), which contained 3.2% sodium citrate, was inserted into the right ventricle; ~10 mL of blood was withdrawn from the animal. Plasma was isolated by centrifugation of the blood for 4 min at 1450×*g* (4 °C) and stored at −30 °C until further experiments. The rats were euthanised via anaesthetic overdose and exsanguination. The samples subjected to electrochemical measurements were prepared in the following way. The plasma containing pazopanib at 10, 50, or 300 μM was obtained by dilution of the 2, 10, or 60 mM pazopanib stock solution 200-fold, respectively. Next, as shown in Figs. 2a and 120 μL of the 300 μM sample was subjected to cyclic voltammetry. Alternatively, as illustrated in Figs. 2b and 100 μL of this sample was mixed by vortexing for 10 s with 400 μL of acetonitrile (Kanto Chemical Co., Inc., Tokyo, Japan), followed by centrifugation for 2 min at 20,000×*g* (4 °C; 'Protocol 1' in Supplementary Fig. S3a). One hundred and 20 μL of the supernatant was subjected to the electrochemical analysis.

The second series of experiments evaluated the repeatability of the measurements by a BDD chip (Fig. 3d) and helped to determine calibration curves for several purposes (Fig. 3b and c and 6; Supplementary Fig. S5, 9, and 10). One hundred microlitres of rat or guinea pig plasma (animal IDs: Rt06−17, GP01−05), which was obtained with the same methods of anaesthesia and sample collection as in the first series above, was mixed by vortexing for 10 s with 0.5 μL of either DMSO alone or a pazopanib stock solution (2, 6, 10, 15, 20, 25, or 30 mM), resulting in plasma samples containing the drug at 0, 10, 30, 50, 75, 100, 125, and 150 μM. Next, each sample was combined with 400 μL of acetonitrile, gently vortexed for 10 s, and centrifuged for 2 min at 20,000×*g* (4 °C). Four hundred microlitres of the supernatant was transferred to a tube that contained 0.4 μL of 10 mM TMA and 0.4 μL of 1 M SDS, followed by vortex mixing for 10 s. One hundred and 20 μL of the sample was then used for electrochemical measurement. These procedures for the spiked samples

are described as 'Protocol 2' in Supplementary Fig. S3b.

In the third series of assays, plasma pazopanib concentrations in rats systemically treated with the drug were measured over time (Figs. 4 and 6; Supplementary Fig. S6 and 7). After adequate anaesthesia by an intra-peritoneal injection of a mixture of 0.375 mg kg^{-1} medetomidine hydrochloride (Kyoritsu Seiyaku Corporation, Tokyo, Japan), 2 mg kg^{-1} midazolam (Sandoz K·K., Tokyo, Japan), and 2.5 mg kg^{-1} butorphanol (Meiji Seika Pharma Co., Ltd., Tokyo, Japan), the right internal jugular vein of rats (n = 9; animal IDs: Rt01−05 and 23−26) was catheterised with a polyurethane blood collection tube (Instech Laboratories Inc., PA, USA) that was filled with heparin-containing saline (heparin sodium; Otsuka Pharmaceutical Factory, Tokushima, Japan). At ≥4 days after the catheterisation, the experiments were conducted as follows. First, whole blood was collected from each rat at 1 h, 30 min, and a few minutes before pazopanib administration. Then, the drug-containing solution (100 mg mL^{-1} kg^{-1} body weight) was given orally to the animals via a feeding needle. In each animal experiment (Fig. 4 and Supplementary Fig. S6 and 7), we monitored the behaviour of the rat for at least 15 min after every drug administration and confirmed that neither vomiting nor leakage of the solution from the mouth occurred. This observation suggested that the dosing was appropriately implemented. The oral administration was followed by longitudinal blood sampling eight times (time points: 1, 2, 3, 4, 5, 6, 8, and 24 h). The sampling amount immediately before the drug administration was 900 μL, which was employed to construct a calibration curve (see also the section '*Calibration curves from rat and guinea pig samples*' below), whereas the amount at other time points was 180 μL. Note that the total amount of blood from each rat did not exceed the limit volume (2.8−3.3 mL) calculated from the guidelines from the European Federation of Pharmaceutical Industries and the European Centre for the Validation of Alternative Methods [68]. Next, the collected blood (900 or 180 μL) was transferred to a polypropylene tube, which in advance contained 100 or 20 μL of a 3.2% sodium citrate solution and was centrifuged for 2 min at 20,000×*g* (4 °C) for plasma isolation. The obtained plasma samples were stored at −30 °C until the electrochemical or LC–MS/MS analyses. Out of nine rats subjected to the above assay, from four rats (animal IDs: Rt23−26), the blood sample was not collected at a certain time point owing to catheter clogging; therefore, these animals were excluded from further analysis. For the other five rats (animal IDs: Rt01−05), the sampling was successful throughout the experiment; however, in three rats (animal IDs: Rt03−05), a sufficient amount of blood for both electrochemical and LC–MS/MS measurements could not be obtained at certain time point(s) owing to our technical errors. Therefore, these plasma samples were analysed only by means of the BDD chip in the tabletop system. Next, the plasma obtained from each rat after the drug administration was thawed; 60 μL of the sample was mixed with 0.3 μL of DMSO and then subjected to the procedures of 'Protocol 2' mentioned above (see three-fifths–scaled procedure in Supplementary Fig. S3b). To build a calibration curve for each of the five rats, standard samples spiked with pazopanib (0−150 μM) were prepared from 60 μL of thawed control plasma and 0.3 μL of the stock solutions. Subsequent preparation of samples was carried out by the procedures of 'Protocol 2' at three-fifths volume scale (Supplementary Fig. S3b). Finally, 120 μL of a sample was employed for electrochemical measurement.

The fourth series of sample preparation procedures was associated with measurements on the handheld disk-shaped device in the portable system (Fig. 7). To construct the calibration curves used in Fig. 7b (see also Supplementary Fig. S12a), test spiked samples containing pazopanib at 0, 10, 30, 50, 75, or 100 μM were prepared from the plasma obtained from a rat (animal ID: Rt18) by the same procedure as in the aforementioned first series. To determine plasma pazopanib concentrations in orally dosed rats (n = 4; animal IDs: Rt19−22; Fig. 7c), ~40 μL of whole blood was collected from the tail vain in each animal without anaesthesia by means of a hematocrit tube (EM MYSTAR Hematocrit Capillary Heparin Treatment; Thermo Fisher Scientific K. K., Tokyo, Japan); the tube was flushed in advance with a 3.2% sodium citrate solution. The obtained blood was immediately transferred to a 0.25 mL microtube (QSP Microtube 503-Q; AS ONE CORPORATION, Osaka, Japan) that already contained 4 μL of the sodium citrate solution and was centrifuged for 2 min at 20,000×*g* (4 °C). Twenty microlitres of the obtained plasma was mixed with 80 μL of acetonitrile by vortexing for 10 s; this sample was next centrifuged for 2 min at 20,000×*g* (4 °C). Eighty microlitres of the supernatant was transferred to a tube containing 0.8 μL of 0.1 M SDS and 0.8 μL of 1 mM TMA, followed by gentle mixing for 10 s. Sixty microlitres of this sample was subjected to the electrochemical measurement with the disk-shaped device. These procedures are designated as 'Protocol 3' in Supplementary Fig. S12b. Note that the calibration curve described in Supplementary Fig. S12c, which was used for calculation of the drug concentrations in the aforementioned rat samples, was built beforehand on the basis of the commercially available rat plasma (Rockland Immunochemicals, Inc., Philadelphia, PA, USA) that was spiked with different amounts of pazopanib (0−100 μM).

Sample types for the experiments with pazopanib were listed in Supplementary Table S3, which also provides the information of the assays with other drugs (see below).

5.5. Preparation of rat plasma samples containing lenvatinib

The samples containing lenvatinib at different concentrations were prepared as follows (Supplementary Fig. S13b). The 0.1, 0.3, 1.0, and 3.0 mM stock solutions were diluted 1000-fold with the plasma that was collected from a rat in the aforementioned first series of experiments for pazopanib detection, by 1000-fold to prepare test spiked samples of 0.1, 0.3, 1.0, and 3.0 μM lenvatinib, respectively. An aliquot of 200 μL of each sample was mixed by vortexing for 10 s with 200 μL of acetonitrile, followed by centrifugation for 2 min at 20,000×*g* (4 °C). One hundred and 50 μL of the supernatant was transferred to a microtube containing 0.3 μL of 10 mM TMA and 150 μL of PBS, followed by vortex mixing for 10 s. After that, 120 μL of the supernatant was assayed with the BDD chip in the tabletop system.

5.6. Preparation of rat plasma samples containing doxorubicin

The samples containing doxorubicin at different concentrations were prepared as follows (Supplementary Fig. S13e). The 3, 10, 30, 100, 300, and 500 μM stock solutions were diluted 1000-fold with the commercially available rat plasma (Rockland

Immunochemicals, Inc., Philadelphia, PA, USA) by 1000-fold to prepare test samples of 3, 10, 30, 100, 300, and 500 nM, respectively. An aliquot of 100 μL of each sample was vortexed for 10 s with 400 μL of acetonitrile, followed by centrifugation for 2 min at 20,000×*g* (4 °C). A total of 400 μL of the supernatant was transferred to a microtube containing 0.4 μL of 1 M SDS and 0.4 μL of 1 mM TMA, followed by vortex mixing for 10 s. Finally, 120 μL of the supernatant was assayed with the BDD chip in the tabletop system.

5.7. Calibration curves from rat and Guinea pig samples

Current amplitudes at −0.45 and −0.35 V were extracted from SWS voltammograms of a rat or guinea pig test plasma sample at each pazopanib concentration (0, 10, 30, 50, 75, 100, 125, and 150 μM). Then, from these two datasets, the slope ($\Delta I/\Delta V_{-0.35\ V;-0.45\ V}$) was calculated and plotted as a function of drug concentration. It must be pointed out that in some experiments, all the $\Delta I/\Delta V_{-0.35\ V;-0.45\ V}$ values (pazopanib: 0–150 μM) determined in five rats were plotted in a single graph and analysed to compute the 'general' slope (Supplementary Fig. S6b; animal IDs: Rt01−05). For the calibration curve of lenvatinib (Supplementary Fig. S13c), $\Delta I/\Delta V_{-0.35\ V;-0.45\ V}$ values at 0, 0.1, 0.3, 1.0, and 3.0 μM from the SWS voltammograms were used and plotted as a function of the concentration. The data were fitted to a four-parameter logistic-regression model.

In each series of analyses, the data were fitted to a linear or nonlinear regression function in GraphPad Prism 9 (GraphPad Software, San Diego, CA, USA).

5.8. Construction of the portable system

A prototype of a handheld disk-shaped drug-monitoring device was constructed from several components by EC Frontier Co., Ltd. (Kyoto, Japan); the blueprint is shown in Supplementary Fig. S11. The device was assembled from inner and outer containers that were composed of polychlorotrifluoroethylene and aluminium, respectively. The disk-type inner container (diameter: 50 mm, height: 21 mm) encompassed a cylindrical chamber (diameter: 3.5 mm, height: 5.5 mm, and volume: 52.9 μL) that housed a small plate-type BDD electrode chip (∼1 × ∼1 cm) at the bottom. The area of the electrode surface immersed in a drug-containing solution was 9.6 mm^2. The electrode chip was underlaid by a brass disk that was connected to a smartphone-sized potentiostat (pocketSTAT: 115 × 59 × 13 mm; Ivium Technologies B·V., Eindhoven, Netherlands) via a copper wire. The applied potential accuracy and measured current accuracy of this potentiostat are ±2 mV and ±0.2%, respectively, which are basically similar to those of the potentiostat in the tabletop system (±1 mV and ±0.2%, respectively), in accordance with the product specifications. A counter electrode (platinum) and reference electrode (Ag/AgCl) were inserted into the cylindrical chamber. The top of the chamber was attached to a conical cavity (depth: 6 mm, large diameter: 15.5 mm) that was designed to facilitate sample application. The inner container was encased with the outer container made of aluminium. The electrochemical measurements were performed by the same potential protocol as shown in Fig. 3a; the protocol consisted of four procedures (see section '*Electrochemical measurements*' above).

5.9. Pharmacokinetics

Pharmacokinetics of pazopanib in the plasma of each rat dosed with the drug were evaluated by means of three parameters, which were extracted from the electrochemical data (Table 2). First, the highest concentration among the blood-sampling time points was designated as $C_{max,obs}$. The second parameter was $t_{max,obs}$, which is the time elapsed before the concentration reached $C_{max,obs}$. The third parameter was AUC_{8h}, i.e. the area under the curve at time points '0 h' to '8 h'. AUC_{8h} was determined in GraphPad Prism 9.

5.10. Collection and analysis of clinical samples

The study for evaluation of a BDD chip with clinical samples was designed in accordance with the Helsinki Declaration (1964, amended in 2000) of the World Medical Association and was approved by the Institutional Review Board of Niigata University (approval No. 2018-0234). This observational study was conducted at the Department of Medical Oncology, Niigata University Medical and Dental Hospital (Niigata, Japan).

Between October 2018 and September 2020, eight patients with soft tissue sarcoma, who were older than 18 years and were treated with pazopanib, were found to be eligible for the study. Thus, four male and four female patients (IDs: Pt01–Pt08) were enrolled; the median age was 66 years (ranging from 23 to 76 years). After agreeing with the purpose and procedures of the study and providing written informed consent, all the participants started to receive a single daily oral dose of pazopanib during hospitalisation. In each patient, the dose of pazopanib was determined or changed in accordance with his or her physical condition, age, symptoms of the primary disease, complications, and adverse effects induced by the drug during the monitoring period (drug dose: 800, 600, or 400 mg per day). Note that in two patients (IDs: Pt06 and Pt08), the pharmacotherapy was discontinued due to severe general fatigue and bradycardia, respectively. From participants, whole blood (6 mL for each sampling) was collected via blood collection tubes (2 mL × 3 tubes; Terumo Corporation) containing 3.2% sodium citrate four times as follows: prior to the first drug administration (on the day or the day before; i.e. control or blank samples), 2 h after the first administration, and immediately before the drug administration on Day 3 and 8 (i.e. trough values). As an exception, in one patient (ID: Pt06), the last sampling was carried out on Day 16 because of clinical circumstances. From each patient, an additional amount of blood was collected at some time points for the clinical laboratory tests.

The collected whole-blood samples were centrifuged for 10 min at 1450×*g* (4 °C) to separate plasma. Then, the plasma samples were preserved at −80 °C in a deep freezer until subsequent analysis. The thawed samples were subjected to the electrochemical assays, i.e. construction of calibration curves and estimation of pazopanib concentrations with methods identical to those used for the

animals' samples ('Protocol 2' in Supplementary Fig. S3b and see sections '*Preparation of samples from rat and guinea pig plasma*' and '*Calibration curves from rat and guinea pig samples*' and the *main text*), as well as to the LC–MS/MS analysis (section '*LC–MS/MS*' below). As for Pt05, during the preparation of plasma from the blood obtained before the drug administration, a considerable amount of the sample was lost due to our technical errors. Therefore, this plasma sample underwent only the electrochemical measurements.

Finally, demographic and clinical data were collected from the electronic medical records of the institution.

5.11. Sex of the analysed animals and patients

Pharmacological studies using male and female animals describe gender differences in drug metabolism [66,69]. To stablely monitor pharmacokinetics of pazopanib over time in Fig. 4 and precisely determine pharmacokinetics parameters in Supplemetnary Table S2, we examined only male rats. Next, the experiments with guinea pigs were subjected to evaluation for the performance of the BDD chip but were not designed for pharmacokinetic analysis (Fig. 6). We used both male and female guinea pigs. The analysed samples were plasma, which was collected at a certain time point from deeply anaesthetised animals and subsequently spiked with pazopanib. Therefore, sex differences were unlikely to affect the results. Finally, we exmained the plasma samples from both male and female patients, because within a limited research period we needed to not only enroll appropriate number of the patients but also complete the analysis.

5.12. LODs of electrochemical measurements

An LOD for each experiment with the rats orally dosed with pazopanib was calculated as follows. From SWS voltammetric recordings from the plasma samples, $\Delta I/\Delta V_{-0.35\ V;-0.45\ V}$ values were extracted that were measured three times before the drug administration. Then, the SD of this background signal and the slope of the calibration curve built for an individual animal were used to calculate the LOD via equation [1,70]:

$$LOD = 3SD/slope. \quad (1)$$

In the analysis of clinical samples, the collection of blank blood three times before the drug administration is ethically problematic. Therefore, on the sample obtained once from each patient, SWS voltammetry was performed three times, and the $\Delta I/\Delta V_{-0.35\ V;-0.45\ V}$ values were utilised to determine the LOD via a calibration curve in the same manner as in the rat experiments.

All the LODs are shown in the panels of Figs. 4 and 5 and Supplementary Fig. S7.

5.13. LC–MS/MS

The chemicals used for this analysis – in addition to the reagents from other experiments described above – were as follows: haloperidol, *N*,*N*-dimethylformamide, and formic acid from FUJIFILM Wako Pure Chemical Corporation (Osaka, Japan), and control rat and human pooled plasma with the 3.2% sodium citrate anticoagulant from Japan SLC, Inc. (Shizuoka, Japan) and BioIVT (New York, USA), respectively. A formic acid solution (0.05%) was obtained by diluting 0.5 mL of formic acid with water to a final volume of 1000 mL. Haloperidol, which served as an internal standard (IS), was dissolved in *N*,*N*-dimethylformamide at 1 mg mL^{-1} to prepare a stock solution. This IS was used as the reference for the analyses of human samples. Note that all the rat samples were assayed with the absolute calibration method.

The following solutions were subjected to the LC–MS/MS assays. First, a stock solution of pazopanib (2, 6, 10, 15, 20, 25, or 30 mM in DMSO) was diluted with the control rat pooled plasma to obtain calibration standard (CS) samples of the drug at 0, 1, 3, 10, 30, 50, 75, 100, 125, and 150 μM (100 μL for each). The 0 μM sample was prepared by the addition of 0.5 μL of DMSO to 100 μL of the control plasma. Of these CS samples, 30, 75, and 125 μM solutions also served as quality control (QC) samples that were references for low, medium, and high concentrations, respectively. Each of these CS and QC samples (100 μL) was mixed with 400 μL of acetonitrile by vortexing; after that, the mixture was centrifuged for 5 min at 12,000×*g* (4 °C; CF15R High-Speed Micro Centrifuge; Eppendorf Himac Technologies Co., Ltd., Ibaraki, Japan). These procedures precipitated and removed proteins from the plasma sample. After the centrifugation, the supernatant was collected for further experiments; the volume of each sample subjected to an LC–MS/MS analysis was 1 μL.

To prepare test samples corresponding to the rats dosed with pazopanib, first, an aliquot of 5 μL was taken from the plasma resulting from blood collection at each time point. On several occasions, the volume of the original plasma samples was less than 5 μL; therefore, from these samples, a 1 or 2.5 μL aliquot was withdrawn and diluted 5- or 2-fold with the control rat plasma. In any case, the 5 μL sample solution was treated with 20 μL of acetonitrile as described above in the paragraph about CS and QS samples, and 1 μL of the supernatant was analysed by LC–MS/MS.

The solutions and procedures associated with the analysis of human samples were as follows. The CS samples containing pazopanib at 0, 1, 3, 10, 30, 50, 75, 100, 125, or 150 μM (200 μL each) were prepared by the addition of requisite volume of either DMSO or the pazopanib stock solutions to the control human pooled plasma in accordance with the protocol for the rat samples. The 3 μM, 30 μM, and 100 μM samples served as the QC samples as well. Besides, an IS working solution was obtained via dilution of the stock solution 50,000-fold with acetonitrile (final haloperidol concentration: 20 ng mL^{-1}). A 25 μL aliquot of each CS, QC, and human sample was combined with 100 μL of the IS working solution, and subsequent procedures were the same as those for the rat samples. In this regard, a blank sample was prepared from the control plasma (25 μL) and acetonitrile (100 μL). Finally, 0.5 μL of the supernatant obtained

from each sample was analysed by LC–MS/MS.

The LC was carried out on a Nexera X3 UHPLC system (Shimadzu Corporation, Kyoto, Japan) equipped with a Mastro C18 column (length: 100 mm, inner diameter: 2.1 mm, and particle size: 3 μm; Shimadzu GLC Ltd., Tokyo, Japan) at 40 °C and a flow rate of 0.25 mL min^{-1}. The mobile phase consisted of buffer A: 0.05% formic acid in water, and buffer B: acetonitrile. The chromatography program for the rat plasma samples commenced with 20% of B for 1.5 min, and next, a gradient from 20% to 90% of B was implemented for 5.5 min, the latter composition was maintained for 2 min, and then B concentration was decreased to 20% for 0.1 min and maintained for 2.9 min. For the human plasma samples, the chromatography program commenced with 20% of B for 1 min; then a gradient from 20% to 45% was implemented for 6 min; after that, the B concentration was increased from 45% to 90% for 0.1 min, maintained for 1.9 min, decreased to 20% for 0.1 min, and finally maintained for 2.9 min. MS/MS was performed using a Triple Quad5500 + mass spectrometer (SCIEX; Framingham, MA, USA) with electrospray ionisation. Mass-spectrometric settings were optimised to obtain the maximal signal for each selected reaction-monitoring transition; the determined parameters are provided in Supplementary Table S1. By the multiple-reaction-monitoring method [71], quantitative analysis of pazopanib and haloperidol, that is, the IS, was carried out in negative mode and in positive mode, respectively. In this context, the quantification was based on selected reaction monitoring using the m/z 436 → m/z 224 transition for pazopanib and the m/z 376 → m/z 165 transition for haloperidol.

The LC-MS/MS data were acquired and analysed in Analyst 1.7.2 (SCIEX). The calibration curves for the rat and human plasma samples were built as quantitation plots of the pazopanib peak area in the rat CS samples and those of the peak area ratio of pazopanib/haloperidol in the human CS samples. The curves were fitted to a function by a weighted ($1/x^2$) least-squares linear regression method. The mass-spectrometric signals obtained in the samples from the rats and patients dosed with pazopanib were converted via the calibration curves to analyte concentrations. The lower limit of quantification of pazopanib was 1 μM.

5.14. Statistics

Means ± SD served as descriptive statistics. No power analysis was performed to determine a needed sample size beforehand, but our sample sizes were similar to those generally employed in the field. The statistical methods applied to each series of experiments are mentioned in respective sections of the Results and Methods. In particular, interclass correlation coefficients, ICC(1, 1) and ICC(1, 30), which are associated with Fig. 3d, were computed in SPSS Statistics 22 (IBM, Armonk, NY).

5.15. Information about the BDD chips, animals, and patients

IDs of the BDD chips, animals, and patients analysed in each experiment in this study are listed in Supplementary Table S3. The raw data for this pharmacokinetic analysis are shown in Supplementary Fig. S7a.

Authors' contributions

T.S., G.O., M.M., A.H., Y.S., and H.H. designed the experiments. G.O., S.S., Z.Q., and S.M. developed the experimental setup. K.A. and Y.E. prepared the BDD electrodes and chips. S.S., K.A., O.R., K.W., S.M., and Y.E. helped to establish the protocol for the electrochemical experiments. T.S., G.O., O.R., K.W., and R.K. conducted the electrochemical experiments. T.S., Y.M., M.M., and Y.S. collected the clinical samples. H.N., C.K., R.O., and H.K. designed and conducted the LC–MS/MS experiments. T.S., G.O., S.S., R.O., N. B.A, D.I., H.K., and H.H. analysed the data. T.S., G.O., S.S., N.B.A, D.I., and H.H. wrote the manuscript. All the authors edited the manuscript.

Data availability statement

Data will be made available on request.

Additional information

Supplementary content related to this article has been published online at [URL].

Declaration of competing interest

The authors declare no competing interests.

Acknowledgements

The authors thank Prof. Kazutoshi Nakamura at Niigata University for a valuable suggestion about the statistical analysis and A. Ishii at Osaka University for technical support. This study was partially supported by the following research grants: Grant-in-Aid for Challenging Exploratory Research 20K21883 (to H.H.); Grant-in-Aid for Scientific Research A 18H04062 (to H.H.); AMED-CREST funded by Japan Agency for Medical Research and Development (grant number 21gm1510004 to H.H.); JST Moonshot R&D (grant number JPMJMS2024 to H.H.); Grant-in-Aid for Scientific Research C 22K06695 (to T.S.); Grant-in-Aid for Scientific Research B 21H03805 (to G.O.); Grant-in-Aid for Scientific Research B 18H03513 (to G.O.); a Takeda Science Foundation grant (to G.O.); a

Mochida Memorial Foundation for Medical and Pharmaceutical Research grant (to G.O.); a Fukuda Foundation for Medical Technology grant (to G.O.); a grant from Nishinomiya Basic Research Fund, Japan (to G.O.); a grant from Ichiro Kanehara Foundation for the Promotion of Medical Sciences and Medical Care (to G.O.); a grant from The Naito Foundation (to G.O.); a Yamaguchi Educational and Scholarship Foundation grant (to G.O.); Grant-in-Aid for Young Scientists 20K16005 (to S.S.); Grant-in-Aid for Early-Career Scientists 19K16826 (to Y.M.); Grant-in-Aid for Scientific Research C 20K07842 (to M.M.) and Grant-in-Aid for Scientific Research A 19H00832 (to Y.E.).

Appendix A. Supplementary data

Supplementary data to this article can be found online at https://doi.org/10.1016/j.heliyon.2023.e15963.

References

[1] J.S. Kang, M.H. Lee, Overview of therapeutic drug monitoring, Kor. J. Intern. Med. 24 (1) (2009) 1–10.
[2] S.L. Groenland, R.H.J. Mathijssen, J.H. Beijnen, A.D.R. Huitema, N. Steeghs, Individualized dosing of oral targeted therapies in oncology is crucial in the era of precision medicine, Eur. J. Clin. Pharmacol. 75 (9) (2019) 1309–1318.
[3] M.V. Antunes, R. Linden, P. Schaiquevich, Therapeutic drug monitoring in developing nations: assessing the current state of affairs in South America, Expet Opin. Drug Metabol. Toxicol. 17 (3) (2021) 251–254.
[4] N. Nwobodo, Therapeutic drug monitoring in a developing nation: a clinical guide, JRSM Open 5 (8) (2014), 2054270414531121.
[5] B. Glahn-Martinez, E. Benito-Pena, F. Salis, A.B. Descalzo, G. Orellana, M.C. Moreno-Bondi, Sensitive rapid fluorescence polarization immunoassay for free mycophenolic acid determination in human serum and plasma, Anal. Chem. 90 (8) (2018) 5459–5465.
[6] A. Puscasu, M. Zanchetta, B. Posocco, D. Bunka, S. Tartaggia, G. Toffoli, Development and validation of a selective SPR aptasensor for the detection of anticancer drug irinotecan in human plasma samples, Anal. Bioanal. Chem. 413 (4) (2021) 1225–1236.
[7] M.A. Rashid, S. Muneer, Y. Alhamhoom, N. Islam, Rapid assay for the therapeutic drug monitoring of edoxaban, Biomolecules 12 (4) (2022).
[8] F. Cao, Q. Dong, C. Li, J. Chen, X. Ma, Y. Huang, et al., Electrochemical sensor for detecting pain reliever/fever reducer drug acetaminophen based on electrospun CeBiOx nanofibers modified screen-printed electrode, Sensor. Actuator. B Chem. 256 (2018) 143–150.
[9] X. Wang, Y. Liu, J. Liu, J. Qu, J. Huang, R. Tan, et al., A bifunctional electrochemical sensor for simultaneous determination of electroactive and non-electroactive analytes: a universal yet very effective platform serving therapeutic drug monitoring, Biosens. Bioelectron. 208 (2022), 114233.
[10] H.C. Ates, J.A. Roberts, J. Lipman, A.E.G. Cass, G.A. Urban, C. Dincer, On-site therapeutic drug monitoring, Trends Biotechnol. 38 (11) (2020) 1262–1277.
[11] R. Bruch, C. Chatelle, A. Kling, B. Rebmann, S. Wirth, S. Schumann, et al., Clinical on-site monitoring of ß-lactam antibiotics for a personalized antibiotherapy, Sci. Rep. 7 (1) (2017) 3127.
[12] K. Chang, F. Wang, Y. Ding, F. Pan, F. Li, S. Jia, et al., Development and validation of a novel leaky surface acoustic wave immunosensor array for label-free and high-sensitive detection of cyclosporin A in whole-blood samples, Biosens. Bioelectron. 54 (2014) 151–157.
[13] S.S. Zhao, N. Bukar, J.L. Toulouse, D. Pelechacz, R. Robitaille, J.N. Pelletier, et al., Miniature multi-channel SPR instrument for methotrexate monitoring in clinical samples, Biosens. Bioelectron. 64 (2015) 664–670.
[14] E. Tenaglia, A. Ferretti, L.A. Decosterd, D. Werner, T. Mercier, N. Widmer, et al., Comparison against current standards of a DNA aptamer for the label-free quantification of tobramycin in human sera employed for therapeutic drug monitoring, J. Pharmaceut. Biomed. Anal. 159 (2018) 341–347.
[15] S. Lin, W. Yu, B. Wang, Y. Zhao, K. En, J. Zhu, et al., Noninvasive wearable electroactive pharmaceutical monitoring for personalized therapeutics, Proc. Natl. Acad. Sci. U. S. A. 117 (32) (2020) 19017–19025.
[16] T.M. Rawson, S.A.N. Gowers, D.M.E. Freeman, R.C. Wilson, S. Sharma, M. Gilchrist, A. MacGowan, A. Lovering, M. Bayliss, M. Kyriakides, P. Georgiou, A.E. G. Cass, D. O'Hare, A.H. Holmes, Microneedle biosensors for real-time, minimally invasive drug monitoring of phenoxymethylpenicillin: a first-in-human evaluation in healthy volunteers, Lancet Digit Health 1 (7) (2019) e335–e343.
[17] A. Dasgupta, M.D. Krasowski, Chapter 3 - clinical utility of monitoring free drug levels, in: A. Dasgupta, M.D. Krasowski (Eds.), Therapeutic Drug Monitoring Data, fourth ed., Academic Press, 2020, pp. 27–42.
[18] T. Yano, D.A. Tryk, K. Hashimoto, A. Fujishima, Electrochemical behavior of highly conductive boron-doped diamond electrodes for oxygen reduction in alkaline solution, J. Electrochem. Soc. 145 (6) (1998) 1870–1876.
[19] A. Fujishima, Diamond Electrochemistry, Publisher: Elsevier, 2005.
[20] J. Kozak, K. Tyszczuk-Rotko, M. Wojciak, I. Sowa, M. Rotko, First screen-printed sensor (electrochemically activated screen-printed boron-doped diamond electrode) for quantitative determination of rifampicin by adsorptive stripping voltammetry, Materials 14 (15) (2021).
[21] A. Mueller-Schoell, S.L. Groenland, O. Scherf-Clavel, M. van Dyk, W. Huisinga, R. Michelet, et al., Therapeutic drug monitoring of oral targeted antineoplastic drugs, Eur. J. Clin. Pharmacol. 77 (4) (2021) 441–464.
[22] R.B. Verheijen, H. Yu, J.H.M. Schellens, J.H. Beijnen, N. Steeghs, A.D.R. Huitema, Practical recommendations for therapeutic drug monitoring of kinase inhibitors in oncology, Clin. Pharmacol. Ther. 102 (5) (2017) 765–776.
[23] P. Wang, X. Yuan, Z. Cui, C. Xu, Z. Sun, J. Li, et al., A nanometer-sized graphite/boron-doped diamond electrochemical sensor for sensitive detection of acetaminophen, ACS Omega 6 (9) (2021) 6326–6334.
[24] M. Chiku, T.A. Ivandini, A. Kamiya, A. Fujishima, Y. Einaga, Direct electrochemical oxidation of proteins at conductive diamond electrodes, J. Electroanal. Chem. 612 (2) (2008) 201–207.
[25] E. Popa, Y. Kubota, D.A. Tryk, A. Fujishima, Selective voltammetric and amperometric detection of uric acid with oxidized diamond film electrodes, Anal. Chem. 72 (7) (2000) 1724–1727.
[26] D.A. Tryk, H. Tachibana, H. Inoue, A. Fujishima, Boron-doped diamond electrodes: the role of surface termination in the oxidation of dopamine and ascorbic acid, Diam. Relat. Mater. 16 (4) (2007) 881–887.
[27] R.A. Osteryoung, J. Osteryoung, W.J. Albery, G.T. Rogers, G.B.R. Feilden, G.T. Rogers, et al., Pulse voltammetric methods of analysis, Phil. Trans. Roy. Soc. Lond. Math. Phys. Sci. 302 (1468) (1981) 315–326.
[28] F. Donmez, Y. Yardim, Z. Şenturk, Electroanalytical determination of enrofloxacin based on the enhancement effect of the anionic surfactant at anodically pretreated boron-doped diamond electrode, Diam. Relat. Mater. 84 (2018) 95–102.
[29] J. Grimshaw, Chapter 10 - reduction of carbonyl compounds, carboxylic acids and their derivatives, in: J. Grimshaw (Ed.), Electrochemical Reactions and Mechanisms in Organic Chemistry, Elsevier Science B.V., Amsterdam, 2000, pp. 330–370.
[30] F. Escalona-Duran, P. Villegas-Guzman, E.V. dos Santos, D.R. da Silva, C.A. Martinez-Huitle, Intensification of petroleum elimination in the presence of a surfactant using anodic electrochemical treatment with BDD anode, J. Electroanal. Chem. 832 (2019) 453–458.
[31] K. Westerdijk, I.M.E. Desar, N. Steeghs, W.T.A. van der Graaf, N.P. van Erp, Dutch Pharmacology and Oncology Group (DPOG). Imatinib, sunitinib and pazopanib: from flat-fixed dosing towards a pharmacokinetically guided personalized dose, Br. J. Clin. Pharmacol. 86 (2) (2020) 258–273.
[32] M.N. Roger W Jelliffe, Individualized Drug Therapy for Patients, Academic Press, 2016.
[33] T.K. Koo, M.Y. Li, A guideline of selecting and reporting intraclass correlation coefficients for reliability research, J. Chiropr. Med. 15 (2) (2016) 155–163.

[34] Y. Deng, C. Sychterz, A.B. Suttle, M.M. Dar, D. Bershas, K. Negash, et al., Bioavailability, metabolism and disposition of oral pazopanib in patients with advanced cancer, Xenobiotica; the Fate of Foreign Compounds in Biological Systems 43 (5) (2013) 443–453.
[35] Phamacology review(s) of VOTRIENT, 2010, U.S. Food and Drug Administration, Retrieved December 31, 2022, from https://www.accessdata.fda.gov/drugsatfda_docs/nda/2009/022465s000_PharmR.pdf.
[36] J.M. Bland, D.G. Altman, Statistical methods for assessing agreement between two methods of clinical measurement, Lancet 327 (8476) (1986) 307–310.
[37] T. Bukve, S. Sandberg, W.S. Vie, U. Solvik, N.G. Christensen, A. Stavelin, Commutability of a whole-blood external quality assessment material for point-of-care C-reactive protein, glucose, and hemoglobin testing, Clin. Chem. 65 (6) (2019) 791–797.
[38] C.F. Bowman, J.H. Nichols, Comparison of accuracy guidelines for hospital glucose meters, J. Diabetes Sci. Technol. 14 (3) (2020) 546–552.
[39] A. Fung, M. Knauer, I. Blasutig, D. Colantonio, V. Kulasingam, Evaluation of electrochemiluminescence immunoassays for immunosuppressive drugs on the Roche cobas e411 analyzer [version 2; peer review: 2 approved, 1 approved with reservations, F1000Research (1832) (2017) 6.
[40] R.F. Greene, J.M. Collins, J.F. Jenkins, J.L. Speyer, C.E. Myers, Plasma pharmacokinetics of adriamycin and adriamycinol: implications for the design of in vitro experiments and treatment protocols, Cancer Res. 43 (7) (1983) 3417–3421.
[41] M. Nagahama, T. Ozeki, A. Suzuki, K. Sugino, T. Niioka, K. Ito, et al., Association of lenvatinib trough plasma concentrations with lenvatinib-induced toxicities in Japanese patients with thyroid cancer, Med. Oncol. 36 (5) (2019) 39.
[42] G. Ogata, Y. Ishii, K. Asai, Y. Sano, F. Nin, T. Yoshida, et al., A microsensing system for the in vivo real-time detection of local drug kinetics, Nat. Biomed. Eng. 1 (8) (2017) 654–666.
[43] T. Cajka, O. Fiehn, Toward merging untargeted and targeted methods in mass spectrometry-based metabolomics and lipidomics, Anal. Chem. 88 (1) (2016) 524–545.
[44] A. Nemiroski, D.C. Christodouleas, J.W. Hennek, A.A. Kumar, E.J. Maxwell, M.T. Fernandez-Abedul, et al., Universal mobile electrochemical detector designed for use in resource-limited applications, Proc. Natl. Acad. Sci. U. S. A. 111 (33) (2014), 11984.
[45] A. Taddeo, D. Prim, E.-D. Bojescu, J.-M. Segura, M.E. Pfeifer, Point-of-Care therapeutic drug monitoring for precision dosing of immunosuppressive drugs, J. Appl. Lab. Med. 5 (4) (2020) 738–761.
[46] L. Bian, J. Liang, H. Zhao, K. Ye, Z. Li, T. Liu, et al., Rapid monitoring of vancomycin concentration in serum using europium (III) chelate nanoparticle-based lateral flow immunoassay, Front. Chem. 9 (2021), 763686.
[47] A. Hanawa, G. Ogata, S. Sawamura, K. Asai, S. Kanzaki, H. Hibino, et al., In vivo real-time simultaneous examination of drug kinetics at two separate locations using boron-doped diamond microelectrodes, Anal. Chem. 92 (20) (2020) 13742–13749.
[48] Y.L. Toh, Y.Y. Pang, M. Shwe, R. Kanesvaran, C.K. Toh, A. Chan, et al., HPLC-MS/MS coupled with equilibrium dialysis method for quantification of free drug concentration of pazopanib in plasma, Heliyon 6 (4) (2020), e03813.
[49] J. Jolibois, A. Schmitt, B. Royer, A simple and fast LC-MS/MS method for the routine measurement of cabozantinib, olaparib, palbociclib, pazopanib, sorafenib, sunitinib and its main active metabolite in human plasma, J. Chromatogr., B: Anal. Technol. Biomed. Life Sci. 1132 (2019), 121844.
[50] S. Bilge, B. Dogan-Topal, E.B. Atici, A. Sinag, S.A. Ozkan, Rod-like CuO nanoparticles/waste masks carbon modified glassy carbon electrode as a voltammetric nanosensor for the sensitive determination of anti-cancer drug pazopanib in biological and pharmaceutical samples, Sensor. Actuator. B Chem. 343 (2021), 130109.
[51] A. Paci, G. Veal, C. Bardin, D. Leveque, N. Widmer, J. Beijnen, et al., Review of therapeutic drug monitoring of anticancer drugs part 1 – cytotoxics, Eur. J. Cancer 50 (12) (2014) 2010–2019.
[52] M. Fukudo, G. Tamaki, M. Azumi, H. Shibata, S. Tandai, Pharmacokinetically guided dosing has the potential to improve real-world outcomes of pazopanib, Br. J. Clin. Pharmacol. 87 (4) (2021) 2132–2139.
[53] A. DePalma, Guide to HPLC System Selection, Biocompare, 2021 updated November 5th, 2021. Available from: https://www.biocompare.com/Editorial-Articles/580407-Guide-to-HPLC-System-Selection/.
[54] K. Kim, G.A. McMillin, P.S. Bernard, S. Tantravahi, B.S. Walker, R.L. Schmidt, Cost effectiveness of therapeutic drug monitoring for imatinib administration in chronic myeloid leukemia, PLoS One 14 (12) (2019), e0226552.
[55] D.T. Vithanachchi, A. Maujean, M.J. Downes, P. Scuffham, A comprehensive review of economic evaluations of therapeutic drug monitoring interventions for cancer treatments, Br. J. Clin. Pharmacol. 87 (2) (2021) 271–283.
[56] B.S. Ole Hammerich, Organic Electrochemistry, fifth ed., CRC Press, 2015.
[57] C.E. Sener, B. Dogan Topal, S.A. Ozkan, Effect of monomer structure of anionic surfactant on voltammetric signals of an anticancer drug: rapid, simple, and sensitive electroanalysis of nilotinib in biological samples, Anal. Bioanal. Chem. 412 (29) (2020) 8073–8081.
[58] H. Moriyama, G. Ogata, H. Nashimoto, S. Sawamura, Y. Furukawa, H. Hibino, et al., A rapid and simple electrochemical detection of the free drug concentration in human serum using boron-doped diamond electrodes, Analyst 147 (20) (2022) 4442–4449.
[59] Z. Wu, J. Liu, M. Liang, H. Zheng, C. Zhu, Y. Wang, Detection of imatinib based on electrochemical sensor constructed using biosynthesized graphene-silver nanocomposite, Front. Chem. 9 (2021), 670074.
[60] A. Cetinkaya, S.I. Kaya, G. Ozcelikay, E.B. Atici, S.A. Ozkan, A molecularly imprinted electrochemical sensor based on highly selective and an ultra-trace assay of anti-cancer drug axitinib in its dosage form and biological samples, Talanta 233 (2021), 122569.
[61] Attached materials for manufacturing and marketing approval application form (Report number: CD2002/00063/00), 2012, Pharmaceuticals and Medical Devices Agency, Retrieved December 31, 2022, from https://www.pmda.go.jp/drugs/2012/P201200143/index.html.
[62] T.A. Ivandini, T.N. Rao, A. Fujishima, Y. Einaga, Electrochemical oxidation of oxalic acid at highly boron-doped diamond electrodes, Anal. Chem. 78 (10) (2006) 3467–3471.
[63] A. Suzuki, T.A. Ivandini, K. Yoshimi, A. Fujishima, G. Oyama, T. Nakazato, et al., Fabrication, characterization, and application of boron-doped diamond microelectrodes for in vivo dopamine detection, Anal. Chem. 79 (22) (2007) 8608–8615.
[64] K.J. French, R.W. Coatney, J.P. Renninger, C.X. Hu, T.L. Gales, S. Zhao, et al., Differences in effects on myocardium and mitochondria by angiogenic inhibitors suggest separate mechanisms of cardiotoxicity, Toxicol. Pathol. 38 (5) (2010) 691–702.
[65] L. Zhang, H. Wang, W. Li, J. Zhong, R. Yu, X. Huang, et al., Pazopanib, a novel multi-kinase inhibitor, shows potent antitumor activity in colon cancer through PUMA-mediated apoptosis, Oncotarget 8 (2) (2017) 3289–3303.
[66] J.C. Fuscoe, V. Vijay, J.P. Hanig, T. Han, L. Ren, J.J. Greenhaw, et al., Hepatic transcript profiles of cytochrome P450 genes predict sex differences in drug metabolism, Drug Metabol. Dispos. 48 (6) (2020) 447–458.
[67] C. Kilkenny, W.J. Browne, I.C. Cuthill, M. Emerson, D.G. Altman, Improving bioscience research reporting: the ARRIVE guidelines for reporting animal research, PLoS Biol. 8 (6) (2010), e1000412.
[68] K.H. Diehl, R. Hull, D. Morton, R. Pfister, Y. Rabemampianina, D. Smith, et al., A good practice guide to the administration of substances and removal of blood, including routes and volumes, J. Appl. Toxicol. 21 (1) (2001) 15–23.
[69] B.H. Shapiro, A.K. Agrawal, N.A. Pampori, Gender differences in drug metabolism regulated by growth hormone, Int. J. Biochem. Cell Biol. 27 (1) (1995) 9–20.
[70] P. Jarujamrus, R. Meelapsom, S. Pencharee, A. Obma, M. Amatatongchai, N. Ditcharoen, et al., Use of a smartphone as a colorimetric analyzer in paper-based devices for sensitive and selective determination of mercury in water samples, Anal. Sci. 34 (1) (2018) 75–81.
[71] K.K. Murray, R.K. Boyd, M.N. Eberlin, G.J. Langley, L. Li, Y. Naito, Definitions of terms relating to mass spectrometry (IUPAC Recommendations 2013), Pure Appl. Chem. 85 (7) (2013) 1515–1609.